Research Article

A Denoising Algorithm Combined with EMD and LMS for Precise Transmission Signal

Lei Song [1], **Yongjun Cao** [2], **Yushan Zhou**,[3] **and Dongdong You** [4]

[1]*School of Mechatronic Engineering, Guangdong Polytechnic Normal University, Guangzhou 510635, China*
[2]*Guangdong Key Laboratory of Modern Control Technology, Guangdong Institute of Intelligent Manufacturing, Guangzhou 510070, China*
[3]*Institute of Automotive Engineering Research, Guangzhou Automobile Group Co., Ltd., Guangzhou 510640, China*
[4]*School of Mechanical and Automotive Engineering, South China University of Technology, Guangzhou 510640, China*

Correspondence should be addressed to Yongjun Cao; 318548571@qq.com

High accuracy and stability in mechanical transmission are crucial for various applications. In spite of the validity of mechanical enhancements, control algorithms' fulfilment offers a cost-effective and efficient approach to mitigating the effects of noise signals. This study presents a hybrid algorithm that combines EMD with the least mean square (LMS) error to achieve online denoising. Within the algorithm, consecutive mean square error (CMSE) and the $\ell 2$-norm metric are employed to assess the similarity between intrinsic mode functions (IMFs) and the original signal; therefore, IMFs are separated into three distinct components: noise components, information components, and mixed components. The denoised signal is obtained by partial reconstruction. Subsequently, the denoised signal is employed as a reference signal in the LMS algorithm, which is utilized for practical processing. The performance evaluation of the developed algorithm employs simulation and experimental signals. The obtained results illustrate that the presented approach achieves sufficient accuracy and stability.

1. Introduction

Precision transmission mechanisms are the core part in intelligent equipment, such as industrial robot and NC machine tools, and its performance is one of the key factors to determine the performance of equipment [1–3]. Traditional mechanical accuracy improvement is the main way to enhance the performance of transmission mechanisms [4, 5]. However, as there are the inherent defects of mechanical improvements, such as high manufacture costs and limited universality, the usage of control algorithm has been drawn attention by researchers.

As the difficulties of mechanical improvement increase, different improvement methods have appeared. Chen et al. [6] found that the measurement error in angle encoders had significant impact to the whole mechanical transmission systems and developed an error model of the encoders, and the error compensation function was applied into RV reducer, in which operation precision was enhanced obviously. Signal acquisition is the precondition in control algorithms, and axial vibration and rotation speed are the main measuring signals in transmission mechanisms; however, these two signals are measured separately, and the synchronization of the two signals becomes a key point in acquisition of transmission mechanism signals. Deng et al. [7] developed a linear array scanning measuring system, and the synchronization of two signals was improved effectively. Torque is one of the key parameters of precision reducer. Yu et al. [8] presented the no-load torque research with motor current signature analysis (MCSA) of signal process approaches. Signals from sensors usually contain noise components, and direct usages of them can bring extra errors into whole systems; for the stability and accuracy, it is necessary to carry out denoising procedure.

Since the empirical mode decomposition (EMD) algorithm is proposed by Huang et al. [9, 10], it becomes

a powerful processing tool for nonlinear and nonstationary signals. Denoising is one of the main operations in the signal process; EMD is able to separate one intact signal into different parts and provide essential convenience to fulfill the denoising process. There are two strategies used in the EMD denoising, one is thresholding and the other is partial reconstruction. Thresholding is a usual denoising strategy, it has been applied in wavelet denoising, and it is reasonable to be transferred to EMD [11, 12]. The EMD partial reconstruction (EMD-PR) is another key tactic for denoising; the indexes to distinguish noise components and information components are the focus of research works [13–15]. Depending on the principle of reconstruction from some stages of IMFs, Boudraa and Cexus [16] proposed the index of consecutive mean square error (CMES), which does not need any prior knowledge for measuring the squared Euclidean distance between two consecutive reconstructions of the signal; the criterion of determining the threshold of CMSE was proposed as well.

Under EMD's inspiration, several time domain decomposition algorithms have been produced out, such as ITD (intrinsic time-scale decomposition), LMD (local mean decomposition), LCD (local characteristic-scale decomposition), VMD (variational mode decomposition), and EWT (empirical wavelet transform), and these algorithms can fulfill similar strategy to EMD for signal process. There are some excellent advantages in these algorithms; for example, the authors of [17, 18] present that ITD has superiorities in robustness and time consumption compared with EMD.

Neither EMD nor other algorithms can process signal online, that is, one of the critical limitations for these algorithms, especially for the precision transmission. Training and conduction are the core ideas of artificial intelligence (AI). The essence of training is information extraction from typical datasets and derivation mathematical models, and the conduction is the application of the model to achieve corresponding targets. These ideas are still suitable for frames of signal processing. Inspiring from this train of thought, the signal processing can be defined into the 2 steps: the first is information extraction and model construction, and the second is conduction of signal process. The first step can be thought as a training process and the second step coincides with the conduction step of AI. The advantages of EMD and algorithms mentioned above are information extraction; they are suitable for the first step, and the next problem is to search an appropriate model for conduction.

Least mean square (LMS) [19] is one of the most adaptive filter algorithms; in the algorithm, the instantaneous error is substituted by MSE (mean square error); the usages of inverse matrix and statistic information are avoided, to be suitable for online processing [20, 21]. Reference signal is indispensable in LMS processing; however, in operations of mechanical equipment, it is difficult to acquire accurate reference signals beforehand. The combination of EMD and LMS can perform their advantages, respectively.

This paper presents a hybrid technique with EMD and LMS, which can denoise the sample signals with EMD algorithm preliminarily and carry out filter process with LMS

algorithm instantaneously. There are three main steps for the presented method: (1) EMD decomposition for sample signals; (2) signals discrimination and reconstruction; and (3) online processing with LMS. In the first step, the sample signals are decomposed into several stages of IMFs with EMD algorithm. In the second step, the IMFs are separated into the following three parts: noise components, information components, and mixed components. To fulfill the separation, two indexes are used in the identification, one is consecutive mean square error (CMSE) and the other is similarity measurement of probability density function (PDF) between IMF and the sample signal, which is expressed as ℓ2-norm. Furthermore, more specific instructions for the two indexes are presented. Different disposal tactics are applied in these three parts, and denoised signals are reconstructed. In the last step, the reconstructed signal is used as reference signal, and LMS algorithm is applied online denoising for measured signal. The simulation signal and the practical RV reducer measuring signal both utilized the presented algorithm.

The remainder of this paper is organized as follows. Section 2 is the brief theory of EMD and LMS. Section 3 introduces the framework of denoising methods developed in this study, and specific steps of the algorithm are illustrated with simulation signal in Section 4. Section 5 presents the experiments for RV reducer transmission measurement and the application of the algorithm. The conclusion and discussion are summarized in Section 6.

2. Basic Theory

2.1. EMD Algorithm. EMD is a kind of time-region signal processing algorithm; it especially fits to analyze nonstationary and nonlinear signal. EMD algorithm uses sifting process for decomposing original signal into several stages of IMF. EMD algorithm can be described as the steps shown in Figure 1.

EMD can decompose a signal into IMFs (intrinsic mode functions), and IMFs satisfy the following two requirements: (1) the difference number between extrema points and zero points is no more than one; (2) the mean of upper envelope and lower envelope is always zero. The decomposition process can be called sifting process, and the properties of EMD, such as completeness, adaptivity, and orthogonality, contribute its advantages for analyzing nonstationary and nonlinear signal.

By decomposing with EMD, the original signal is decomposed into L-1 stages IMFs $h_i(t)$ and one residue $r(t)$. For the convenience of express, residue $r(t)$ is considered as one stage of IMF in this paper, and according to the completeness, the relation between original signal and decomposition results is as follows:

$$S(t) = \sum_{i=1}^{L-1} h_i(t) + r(t) = \sum_{i=1}^{L} \text{IMF}_i(t). \tag{1}$$

End effect and mode mixing are major drawbacks in signal processing with the EMD algorithm. In the sifting process, the end points are treated as extrema, but in fact,
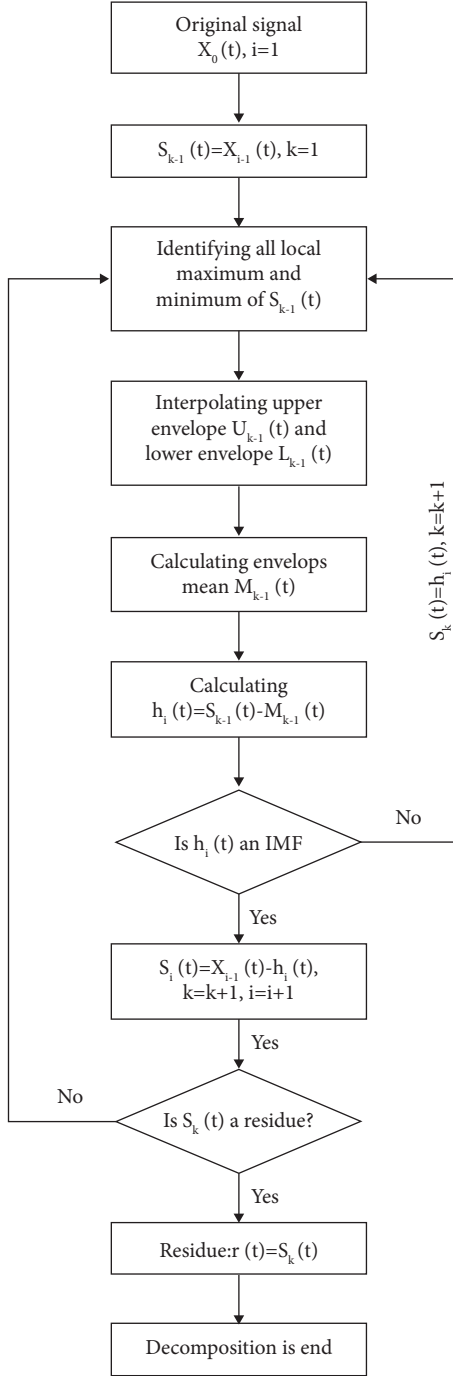
Figure 1: Flow chart of EMD algorithm.

these points are not extrema definitely; therefore, the sifting error will be accumulated and propagated, and eventually, the end effect in sifting is occurred. Mirror extending [22] and sequence prediction [23] are usually used to relieve the end effect. Mode mixing refers to an IMF which contains multiple modes or a mode scatter in different IMFs, and this phenomenon relates with discontinuous change of signal. Mode mixing leads to difficulty for extracting accurate information. For resolving this problem, Wu and Huang [24] introduced a noise-assisted data analysis (NADA) approach, named ensemble EMD (EEMD). The basic procedure of

EEMD is addition of white noise into the signal and then ensemble step will ensure that the effect of addition of white noise is reduced to mean zero statistically. EEMD has achieved the satisfactory results in denoising [25, 26].

2.2. LMS Algorithm. The LMS filter originates from the linear differential model as shown in the following equation:

$$y(n) = \sum_{m=0}^{L-1} w_m(n)x(n-m) = \mathbf{w}^T(n)\mathbf{x}(n), \quad (2)$$

where $\mathbf{x}(n)$ is the signal of input, $y(n)$ is the signal of output, $w_m(n)$ is the weight of the filter, and L is tap-length. Also, the error between reference signal and filter output is defined as follows:

$$e(n) = d(n) - y(n) = d(n) - \mathbf{w}^T(n)\mathbf{x}(n), \quad (3)$$

where $d(n)$ is the reference signal and $e(n)$ is the error between reference signal and filter output $y(n)$. Under the condition of the least mean square error (MSE), the weight matrix is as follows:

$$\widehat{\mathbf{w}} = \mathbf{R}^{-1}\mathbf{P}, \quad (4)$$

where $\mathbf{R}$ is the auto-correlation matrix of input signal $x(n)$, $\mathbf{P}$ is the cross-correlation vector between input signal $x(n)$ and reference signal $d(n)$, and $\widehat{\mathbf{w}}$ is the estimation of weight vector. In the practice, $\mathbf{R}$ and $\mathbf{P}$ are difficult to be acquired, and the optimization criterion of MSE is substituted by instantaneous error square; so, the estimation for gradient can be expressed as the following equation:

$$\frac{\partial[e(n)^2]}{\partial\mathbf{w}} = 2e(n)\frac{\partial[e(n)]}{\partial\mathbf{w}} = -2e(n)\mathbf{x}(n). \quad (5)$$

Deriving from equation (5), the weight vector update equation can be expressed as follows:

$$\mathbf{w}(n+1) = \mathbf{w}(n) - \frac{1}{2}\mu\frac{\partial[e^2(n)]}{\partial\mathbf{w}} = \mathbf{w}(n) + \mu e(n)\mathbf{x}(n), \quad (6)$$

where μ is the step size, and for the convergence of the algorithm, the step size μ should comply with rule as shown in the following equation:

$$0 < \mu < \frac{2}{\lambda_{\max}}, \quad (7)$$
$$0 < \mu < 1,$$

where $\lambda_{\max}$ is the max auto-correlation matrix eigenvalue.

3. Framework of EMD-LMS Denoising Method

In general, EMD algorithm is not able to process the signal online; this is a major limitation in its application. The LMS algorithm is one of the adaptive filter algorithms, and it can fulfill the real-time signal process; however, in the process of this algorithm, the reference signal is the prerequisite, and in most practice situations, difficult determination of accurate

reference signal is the main obstacle for the LMS application. The mode of training and implementation of machine learning is used as reference, and EMD provides powerful processing capacity of training dataset, and LMS fulfils advantages of instantaneous processing; as a result, the combination of EMD and LMS can overcome the respective defects and provide an effective approach for signal denoising process.

The EMD-LMS hybrid approach uses the signal processed by EMD as the reference signal and processes the real-time input signal with LMS. The outline of approach can be described as shown in Figure 2. The specific steps are as follows:

(1) Carry out EMD decomposition with typical signal and acquire the IMFs and residual $r(t)$,

$$S(t) = \sum_{i=1}^{L-1} h_i(t) + r(t) = \sum_{i=1}^{L} \text{IMF}_i(t). \quad (8)$$

(2) Separate IMFs into noise components, mixed components, and information components. The noise components refer to the stages of IMF which is dominated by noise, the mixed components refer to the stages of IMF in which the proportions of noise and information are close, and the information components refer to the stages of IMF which is dominated by authentic signal.

To separate IMFs into 3 parts, the works to measure characteristic of IMFs are essential, and there are two indexes for distinguishing IMFs. In this paper, CMSE and ℓ2-norm are used as key indexes to fulfill IMFs measurement.

(3) Partial reconstruction is carried out regarding as the IMFs distinguishing. Noise components are removed directly, information components are used in reconstruction directly, and the noise and information mixed components should be processed in advance; then, they are used in the reconstruction, and denoising process of reference signal is finished.

(4) The reconstruction result is used as reference signal, and real operation signal inputs the LMS filter to fulfill process. For the LMS algorithm, tap-length is a key parameter; to obtain its optimum, calculate the error of filter and determine the appropriate tap-length.

(5) The real operation signal inputs into the LMS filter and the iteration calculation is carried out, and the denoised signal of real signal is output.

4. Denoising for Simulation Signal

4.1. EMD Process. To present the approach in detail, a simulation signal is introduced. In operation of transmission mechanisms, the signal usually contains vibration signal, fluctuation signal, periodic harmonic signal, and noise signals from different sources. A synthetic signal is given as follows:
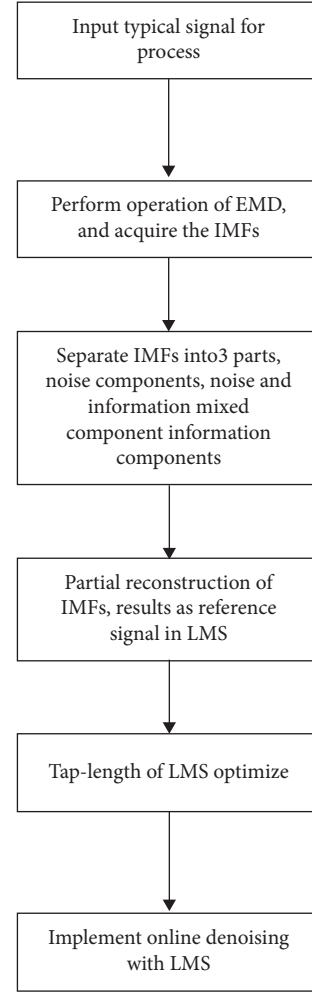

FIGURE 2: The outline of the proposed EMD-LMS hybrid filtering algorithm.

$$S(t) = x_1(t) + x_2(t) + x_3(t) + x_4(t) + x_5(t), \quad (9)$$

where $x_1(t)$ is the modulated signal and can be written as follows:

$$x_1(t) = A_1[a(t)]\cos(2\pi f_m t + \varphi_1), \quad (10)$$

where $a(t)$ is the modulation function; it can be written as follows:

$$a(t) = \sum_{n=1}^{N} A_0 \cos(2\pi n f_r t + \alpha_n). \quad (11)$$

The second component x_2 is the diriclet signal, which represents fluctuation in the process of mechanism rotation; it can be written as follows:

$$x_2(t) = \frac{\text{sinc}[7\pi(t-1)]}{\text{sinc}[\pi(t-1)]}. \quad (12)$$

The third and fourth components both are harmonic signal; it can be written as follows:

$$x_{3,4}(t) = A_{3,4} \sin\left(2\pi f_{3,4} t\right). \qquad (13)$$

Sensor noise is the main effect for control accuracy of mechanical transmission, thermal noise, shot noise, generation-recombination noise, and $1/f$ noise which are the main noise sources in sensors [27]. These noise sources are approximate Gaussian distribution except $1/f$ noise; hence, simulation signals of sensors usually use AWGN (additive white Gauss noise) to simulate noise component in practical situations [28]. The component x_5 is white noise signal. The simulation signals are displayed in Figure 3.

The signal $S(t)$ is decomposed by EEMD, with noise selected at a standard deviation of 0.5 and 200 ensemble number. The decomposition results are shown in Figure 4.

The lower stage IMFs are at higher frequency, and they include more noise components. The higher stage IMFs are at lower frequency, and they include more information components. This characteristic provides a reliable way to reveal the useful information from nonstationary and nonlinear signals. How to distinguish which stages are dominated by noise component and which stages are dominated by information component are the key problems for information extract and filter. For the selection of credibility and certainty, some indexes should be introduced into the analysis for EMD decomposition results.

4.2. CMSE for IMF Discrimination. It can be assumed that as the stage number increases from first to residual, the oscillation frequency of IMF will decrease, and there are less noise components and more information components in IMFs. Based on this assumption, at initial stage, the IMF is dominated by noise components; as the stage increases, the energy of noise components decreases, and the energy of information increases. Eventually, there is a certain stage number of IMF, and the energy of information components transcends the noise. Behind this certain stage, the IMFs are dominated by information components. Boudraa and Cexus [16] developed consecutive mean square error (CMSE); it is derived from signal estimation index and mean square error (MSE). In the MSE, the authentic signal should be acquired in advance, but in the signal denoising and estimation, it is difficult to obtain the authentic signal beforehand, and MSE cannot be used in the process directly. CMSE presents an effective approach to measure the squared Euclidean distance between the two signals. The CMSE is defined as follows:

$$\mathrm{CMSE}\left(\tilde{y}_k, \tilde{y}_{k+1}\right) = \frac{1}{N} \sum_{j=1}^{N} \left[\tilde{y}_k(t_j) - \tilde{y}_{k+1}(t_j)\right]^2$$

$$= \frac{1}{N} \sum_{j=1}^{N} \left[\mathrm{IMF}_k(t_j)\right]^2, \qquad (14)$$

where the $\tilde{y}_k$ is indicated as follows:

$$\tilde{y}_k = \sum_{i=k}^{L-1} h_i(t) + r(t) = \sum_{i=k}^{L} \left[\mathrm{IMF}_i(t)\right]. \qquad (15)$$

According to the characteristic of the IMFs distribution, the initial stage of IMFs is almost noise components, and as the stage increases, the noise components will decrease, and the CMSE will decrease. When the decrease of noise components reaches a certain level, the CMSE will reach at local minimum. After this local minimum, the information components will increase. So, the variance of CMSE value can indicate the variance of proportion between noise and information components. According to the presentation in [16], the criterion of cut-off point is defined as follows:

$$M_1 = \operatorname*{arg\,min}_{1 \leq k \leq L-1}\left[\mathrm{CMSE}\left(\tilde{y}_k, \tilde{y}_{k+1}\right)\right]. \qquad (16)$$

The developed approach in this paper separates IMFs into 3 parts, the authors of [16] use equation (16) to separate IMFs into 2 parts, and if equation (16) is used directly as the criterion of cut-off point in the presented approach, it will lead to contradiction. Usually, there are several local minimums of CMSE; equation (16) neglects fluctuation of proportion between noise and information components. Because noise components mainly exist in initial stages of IMFs, the first local minimum using as cut-point would be more reasonable. This paper adjusts the criterion of CMSE into the following expression:

$$M_1 = \operatorname*{arg\,first\,local\,min}_{1 \leq k \leq L-1}\left[\mathrm{CMSE}\left(\tilde{y}_k, \tilde{y}_{k+1}\right)\right]. \qquad (17)$$

This criterion brings the M_1 forward and recognizes less stages as noise signals; meanwhile, some IMFs mixed with noise components and information components are retained in remaining IMFs; it is necessary to deal with these IMFs. Comparing with equation (16), the selected-out noise IMFs decrease and the accuracy is improved consequently.

The CMSE fluctuation of simulation signal is shown in Figure 5. In the plot, the CMSE reaches the first local minimum at the 3rd stage, according to equation (16), the IMFs of 1–3 stages are dominated by noise, and these three stages of IMFs can be removed in the reconstruction.

4.3. ℓ2-Norm for IMF Discrimination. CMSE can select out the IMFs dominated by noise components, there are still some stages of IMFs mixed with noise components and information components, and other stages of IMFs are dominated by information components. At the end stages of IMFs, they are dominated by information components; so, they are more similar with original signal than initial stages of IMF, and it is reasonable to consider the higher stages of IMF which are dominated by information components.

The probability distribution function (PDF) represents the data distribution shape of signal, PDF can provide more robust and accurate metric for measuring similarity than signal dataset of time domain. Geometric indexes are usually used to measure quantity characterization of the similarity, and ℓ2-norm is suitable to express Euclidean distance between two datasets. P_0 and P_1 are assumed as PDFs of two signals, respectively, and the ℓ2-norm can be written as follows:
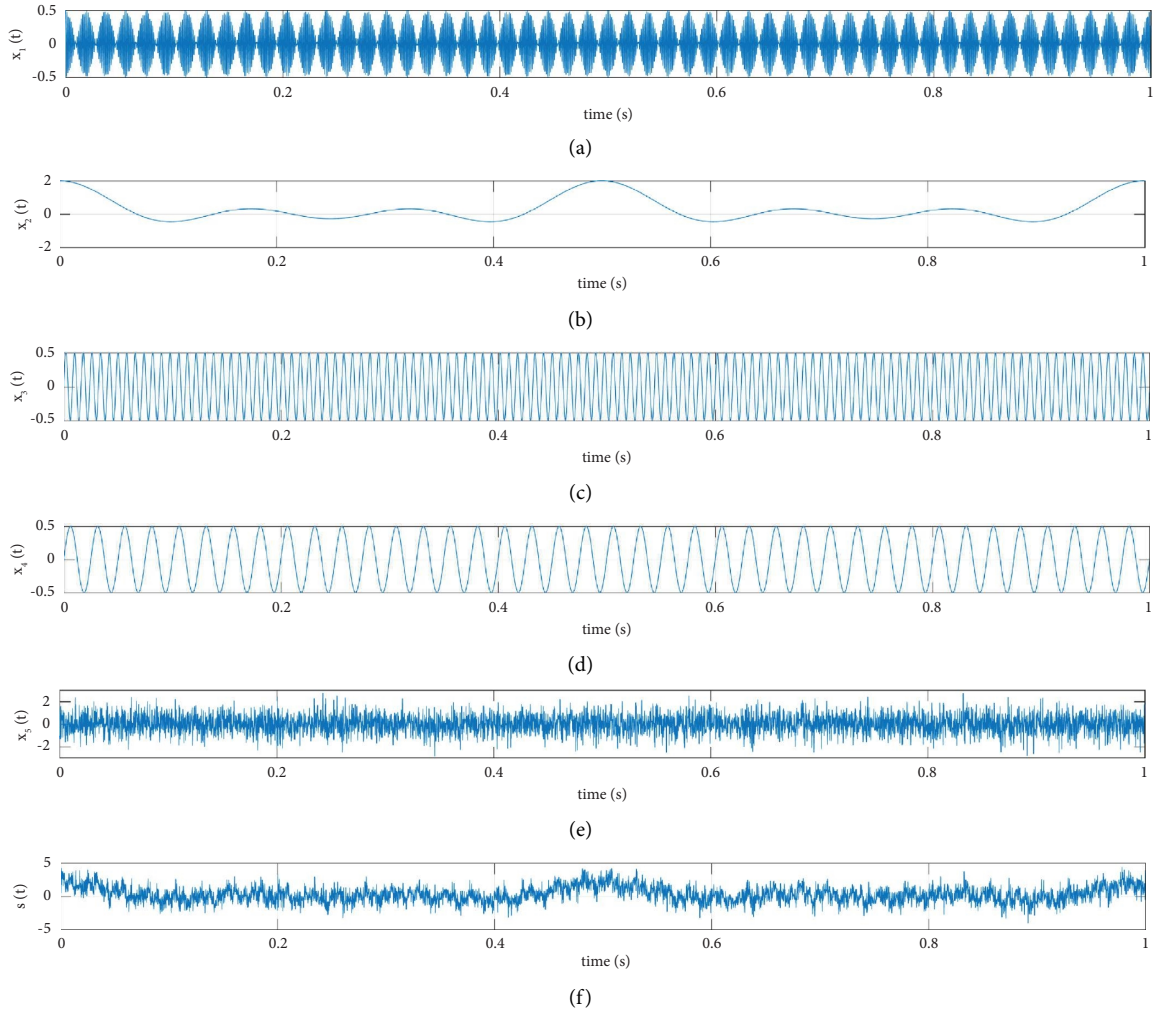
FIGURE 3: The plot of simulation signal. (a) The component $x_1(t)$, (b) the component $x_2(t)$, (c) the component $x_3(t)$, (d) the component $x_4(t)$, (e) the component $x_5(t)$, and (f) the synthetic signal $S(t)$.

$$\left\| P_0 - P_1 \right\|_2 = \left\{ \int_{-\infty}^{+\infty} \left[P_0(y) - P_1(y) \right]^2 dy \right\}^{1/2}. \qquad (18)$$

According to the $\ell2$-norm, the similarity between the original signal and each stage of IMF can be calculated by the following equation:

$$\text{dist}\left(P_s, P_{\text{IMF}i}\right) = \text{norm}_{\ell_2}(i) = \left\| P_s - P_{\text{IMF}i} \right\|_2 = \left\{ \int_{-\infty}^{+\infty} \left[P_s(y) - P_{\text{IMF}i}(y) \right]^2 dy \right\}^{1/2}, \qquad (19)$$

where $P_s(y)$ is the PDF of original signal and $P_{\text{IMF}i}(y)$ is the PDF of the IMF of No. i stage. The stage number selected for cut-off point usually is defined as follows:

$$M_2 = \underset{1 \leq k \leq L}{\arg\max} \left[\text{dist}\left(P_s, P_{\text{IMF}i} \right) \right] = \underset{1 \leq k \leq L}{\arg\max} \left\{ \int_{-\infty}^{+\infty} \left[P_s(x) - P_{\text{IMF}i}(x) \right]^2 dy \right\}^{1/2}. \qquad (20)$$
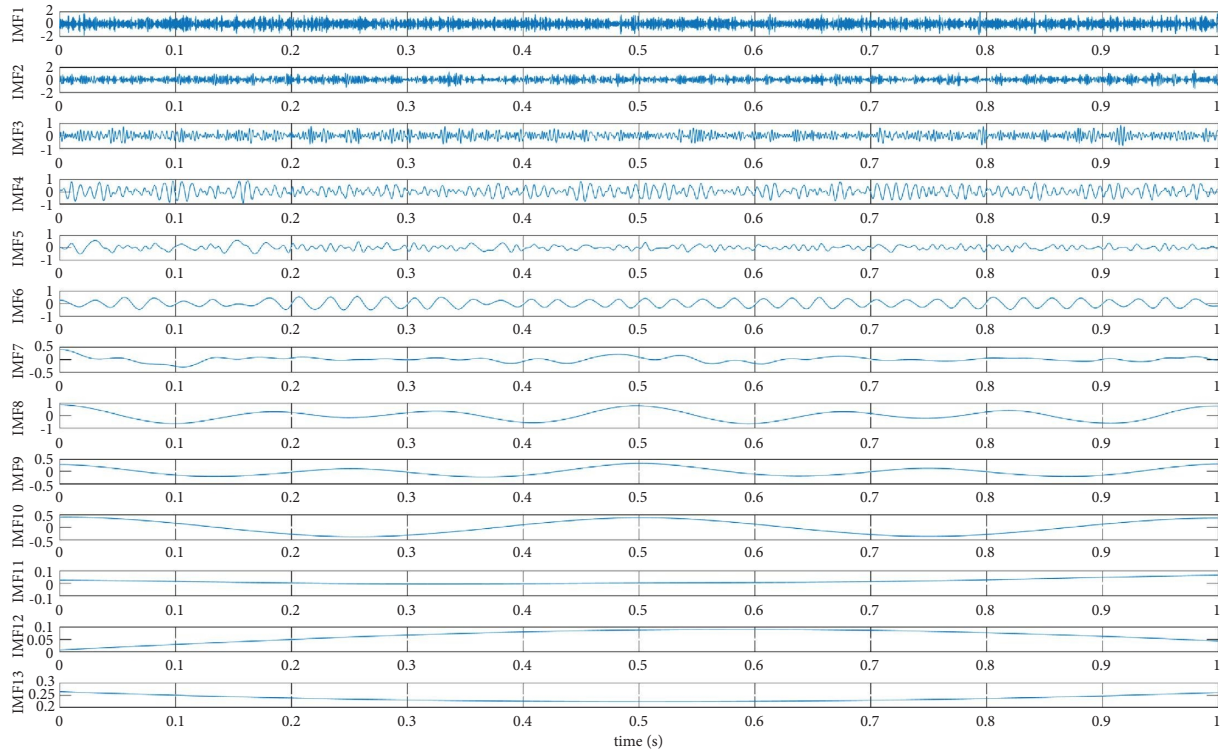
FIGURE 4: EEMD decomposition results of the simulated signal $S(t)$.
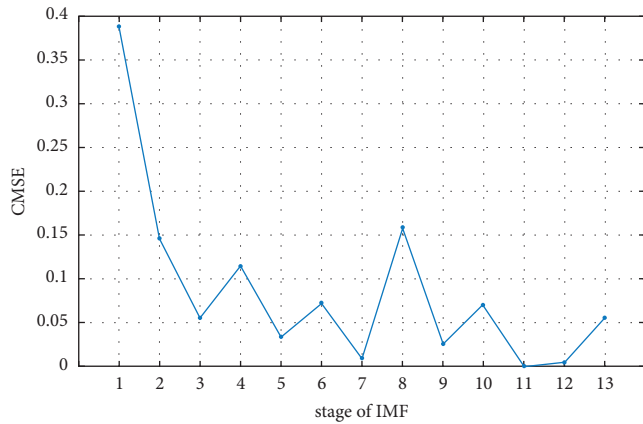
FIGURE 5: The diagram of CMSE index of simulation signal.

For some signals, their M_2 index is too large, approximate or even equal to the last stage. In practice, the IMFs of the last three stages are dominated by information components; so, the M_2 should not be more than L-3. The selection process is shown in Figure 6.

The PDF comparison between simulation signal and respective IMF is shown in Figure 7. The ℓ2-norm of simulation signal is shown in Figure 8. In the diagram, there are 3 local maximum points. Although the IMF of the last stage is the global maximum, its stage does not conform to the criterion of being less than L-3, and the last stage is excluded according to the judge criterion. The first local maximum of ℓ2-norm is at the IMF of the 2nd stage, the second local maximum at the IMF of the 6th stage, and the

third local maximum is at the IMF of the 9th stage. The third local maximum is the largest and it conforms the criterion of being less than L-3; so, the parameter M_2 can be determined as 9.

IMFs from 1 to M_1 stages are considered as noise components and should be removed in the process of reconstruction. IMFs from $M_1 + 1$ to M_2 are considered as components mixed with noise and information, and after being denoised, these IMFs can be used in the reconstruction process components. IMF stages from M_2 to the last are considered as information components and can be used in the process of reconstruction directly.

4.4. Testifying Validity of IMF Selection Indexes.

Above the context, the selection approaches of M_1 and M_2 are presented. These indexes separate IMFs into the following three parts: noise components, mixed components, and information components. For ensuring accuracy of denoising results, it is necessary to testify the feasibility and validity of M_1 and M_2 indexes. The energy of signal is usually used in reviewing the selection effectiveness of signal [29, 30].

The IMF dominated by noise components are of different trend with IMFs dominated by information components. As the stage increases, the distinction between energy of IMFs and corresponding noise signal will expand. Energy comparison between noise signal and the actual IMFs can be used in testifying the validity of parameter selection. In this analysis approach, how to calculate noise-only signal is a tricky problem. According to characteristic of EMD, the IMF of the first stage can be assumed as noise-only
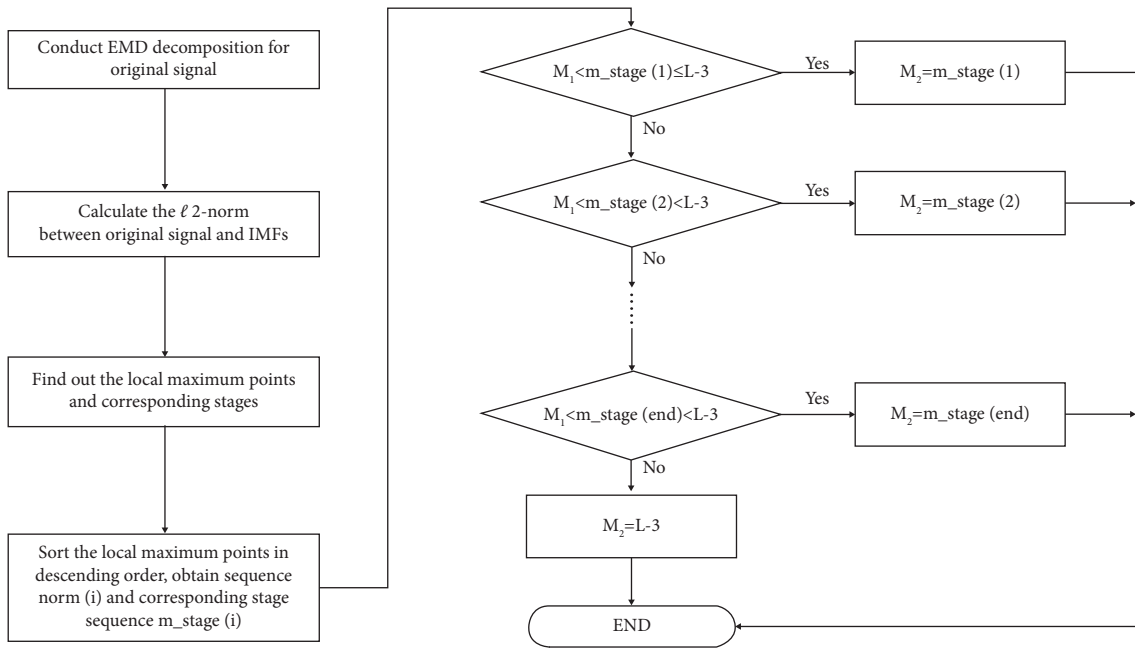
FIGURE 6: The process of determination parameter M_2.
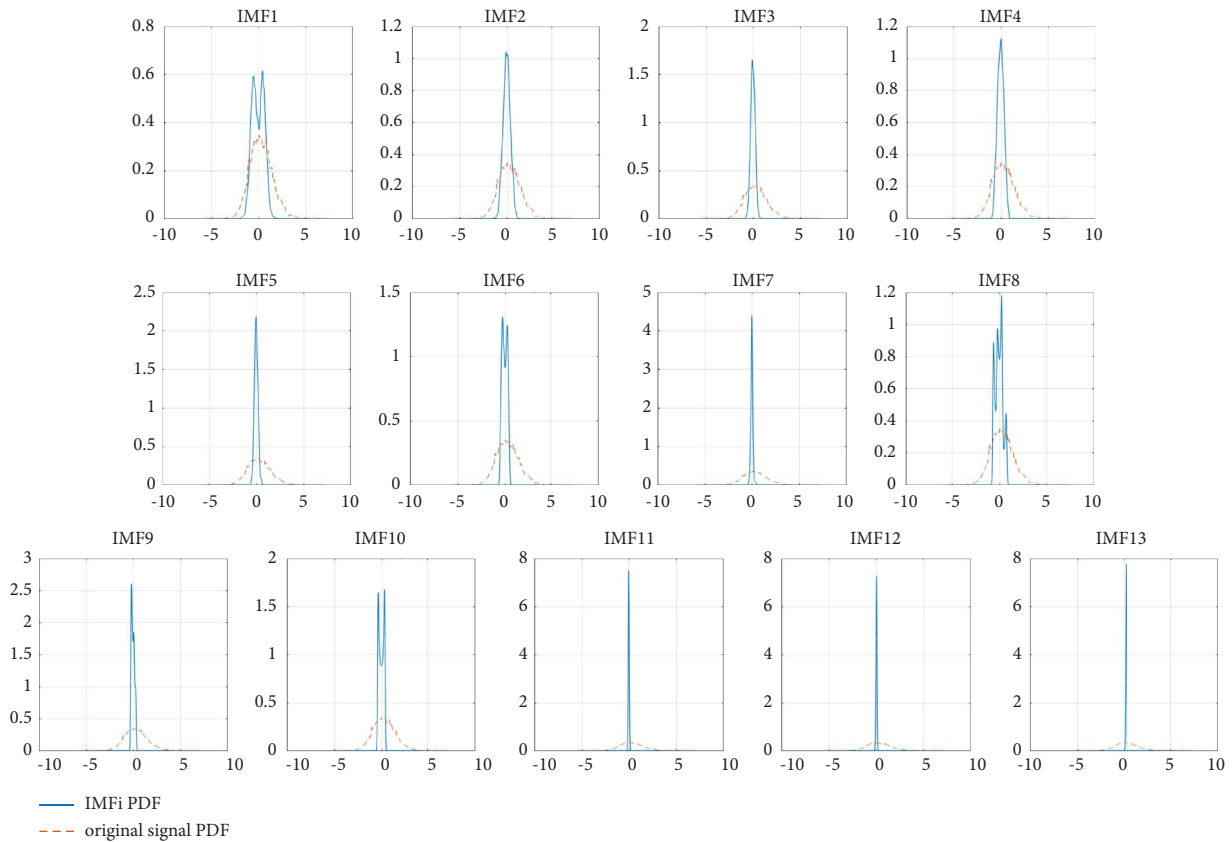
FIGURE 7: The diagram of PDF of original signal and IMF.
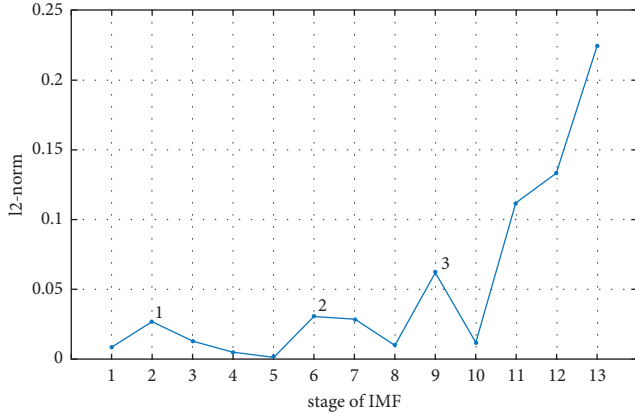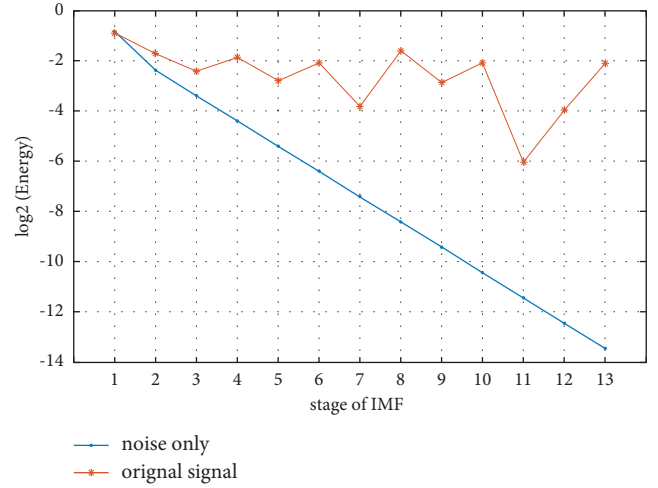
FIGURE 8: The diagram of $\ell 2$-norm of simulation signal.

FIGURE 9: Energy comparison between theoretical noise-only signal and original signal with respect to the corresponding stage number of IMF.

signal. As Hurst exponent is 0.5, the noise signal will be the Gauss white noise, and its mean is zero, the variance could represent the energy of noise signal. The energy of the first IMF can be calculated as follows:

$$E_1 = \hat{\sigma}_1^2, \tag{21}$$

where $\hat{\sigma}_1$ is the variance of the IMF of the first stage. Mallat [31] proposed an effective calculation approach as shown in the following equation:

$$\sigma_1 = \frac{\text{median}\left(\left|\text{IMF}_1(t)\right|: t = 1, 2, \cdots, N\right)}{0.6745}, \tag{22}$$

where N is the length of signal.

The energy of subsequent stage in noise-only signal can be estimated by equation (23) proposed by Flandrin et al. [32], which presents an effective approach to acquire the energy of subsequent stages.

$$\widehat{E}_k = C_H \rho_H^{-2(1-H)k}, \tag{23}$$

where C_H can be defined as follows:

$$C_H = \frac{E_1}{\beta}. \tag{24}$$

In the equation, H is the Hurst exponent, and its value is 0.5. Under this condition, the noise signal is Gauss white noise, and the parameters β and ρ are 0.719 and 2.01, respectively, according to [32].

Energy comparison between theoretical noise-only IMFs and actual IMFs of the original signal is shown in Figure 9. In the diagram, the IMFs energy of original signal IMF from 1 to 3 stages is very close to energy of the theoretical noise-only, and it is reasonable to discard the IMF from 1 to 3 stages as noise signal in the denoise process. From 4 to the end stage, the energy of IMF starts to diverge the noise-only signal, but the deviation is fluctuant around the theoretical line. It can be concluded that noise components in IMFs after the 3rd stage reduce and information components increase. At the last, in a few stages, the deviation is enlarging, and it can be concluded that these stages are dominated by information components. Comparing the

current results with M_1 and M_2, M_1 coincides the current result and M_2 is not equal to the current results exactly but is close. Considering the accuracy fluctuation of energy approach, the approach presented in this paper is close to the actual situations, and the effectiveness is testified.

According to the calculation results of M_1 and M_2, IMFs from 1 to 3 are dominated by noise, they are wiped off directly, IMFs from 4 to 9 stages are mixed with information and noise, the further process is needed for denoising the noise components, and the IMFs from 10 to the last can be used in reconstruction directly.

4.5. Signal Part Reconstruction.

Kalman filter (KF) is an effective approach to estimate instantaneous state of a linear dynamic system contaminated with noise signal, and it can achieve the statistical optimum with respect to quadratic function of estimator error.

As Kalman filter is used in denoising, actually the algorithm estimates the current value under the involvement of noise, the process mainly includes two steps, presented as follows:

(1) Predicting the current state value and error covariance derived from the previous state value

(2) Correcting the current state value and error covariance derived from the predicting value and the measurement value

The KF is applied for denoising the IMFs stage from stages 4 to 9, IMFs mixed with information, and noise components; the results are shown in Figure 10. According to the diagram, the KF can restrain the noise components of IMFs.

The IMFs from 1 to 3 stages are noise components, they are wiped off directly in reconstruction, the IMFs from 4 to 9 stages are mixed components, KF filtering results can be used in reconstruction, and the IMFs from 10 to 13 stages can be used in reconstruction directly. The result of
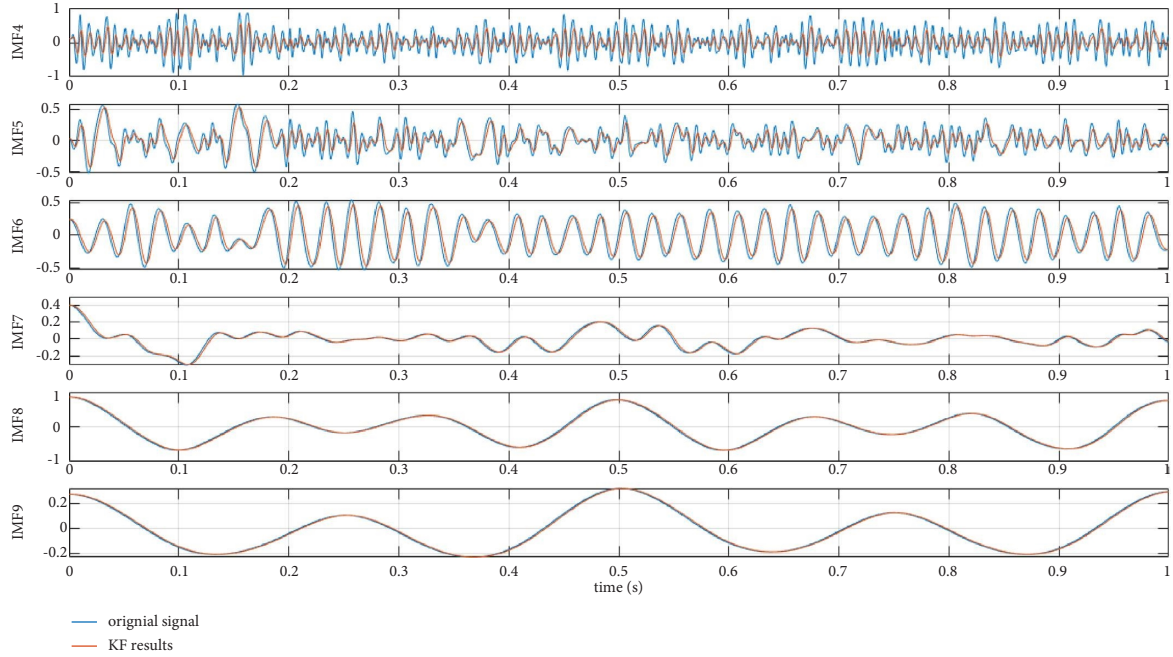
FIGURE 10: The diagram of KF filter results of IMFs from 4 to 9 stages.

reconstruction is shown in Figure 11, and $S_f(t)$ is the signal filtered through original simulation signal $S(t)$. The reconstruction signal restrains the noise components in original signal effectively, the signal-noise-ratio (SNR) of signal is enhanced from 1.60 to 6.49.

4.6. Simulation Signal Denoising with LMS. The reconstruction signal can be regarded as the reference signal and then online simulation signal can be denoised by the LMS algorithm. The tap-length is a key factor to affect the calculation consumption and stability, and it is necessary to determinate appropriate tap-length. In this paper, the MSE is used as index to depict the optimality of tap-length. Figure 12 displays the MSE variation with the tap-length. When the tap-length is 2, the MSE of LMS output is 0.25, as the tap-length is increasing, the MSE is decreasing. When the tap-lengths have increased around 20, the MSE will decrease slowly; consequently, tap-length can be evaluated as 20.

In LMS processing, step size is a key parameter for the stability and rate of convergence; therefore, variable step size becomes an effective action to achieve better results. Normalization is a useful processing to improve stability of the algorithm [33], and in LMS, the step size normalization can be defined as follows:

$$\mu(n) = \frac{\mu}{\|x(n)\|_2^2}, \tag{25}$$

where μ is the initial step size of LMS and $x(n)$ is the value of input signal of LMS at nth time.

Sigmoid function is one of the most universal approaches for step size adaptive adjustment [34], and it can be expressed in the following equation:

$$\mu(n) = b\left(\frac{1}{1 + e^{-a|e(n)|}} - \frac{1}{2}\right), \tag{26}$$

where a and b are positive constants and $e(n)$ is the LMS error at nth time.

To achieve a better effect, normalization and sigmoid function are combined as follows:

$$\mu(n) = b\left(\frac{1 - e^{-a|e(n)e(n-1)|}}{r + \|x\|_2^2}\right), \tag{27}$$

where r is constant from 0 to 1. In this paper, equation (27) is applied in LMS processing.

The simulation signal $S(t)$ is used as input signal, the denoised signal $S_f(t)$ is used as reference signal, and the tap-length is 20. The processed signal by LMS algorithm is shown in Figure 13. The SNR of LMS output is 5.72; the effect of denoising is improved further.

4.7. Comparison with Related Algorithms. Wavelet thresholding, EMD-IT (EMD interval thresholding) and EMD-PR (EMD part reconstruction) are the main algorithms for nonstationary signal denoising, and comparisons between them and presented in this paper are carried out, and for the consistency, EEMD is applied in EMD-IT and EMD-PR. The denoising results of simulation signals with wavelet thresholding, EEMD-IT, and EEMD-PR are shown in Figure 14. The accuracy of denoised results comparison is shown in Table 1. The simulations are performed on the MATLAB (2020a) that is installed on a computer with 1.8 GHz Intel Core i7-8550, 16 GB RAM, and the comparisons of calculation time cost are shown in Table 2.
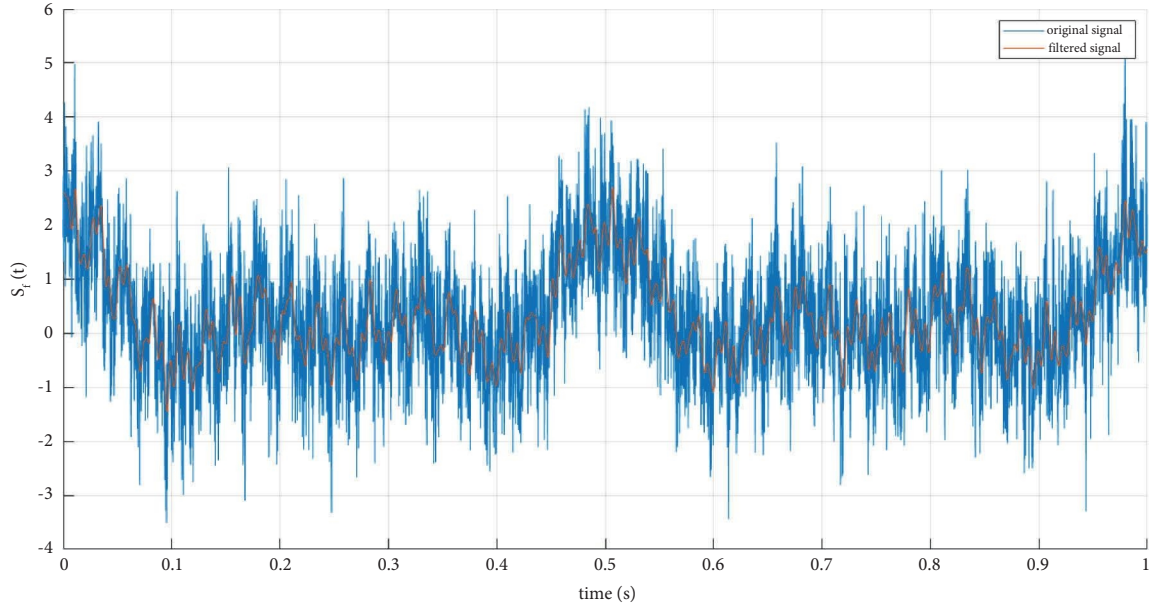
FIGURE 11: The diagram of signal of reconstruction.
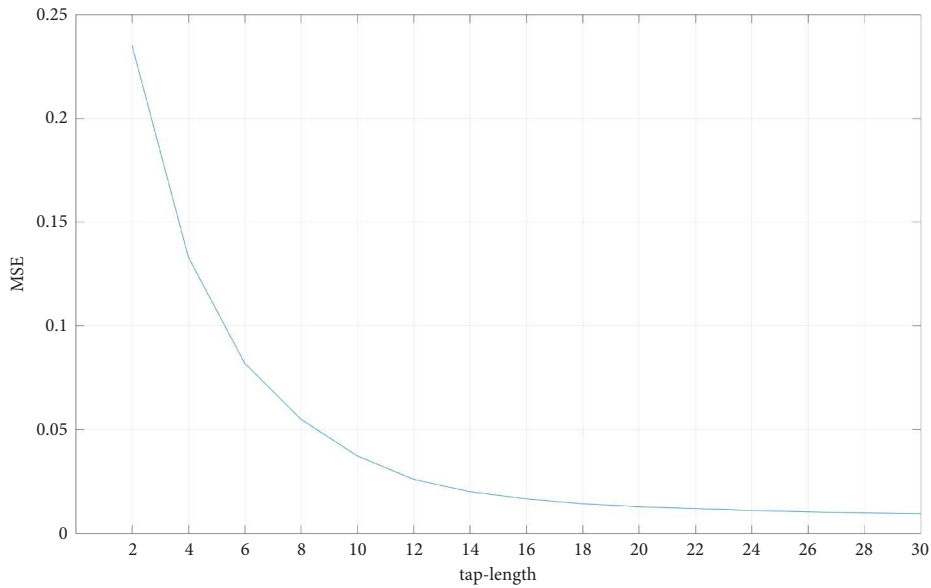
FIGURE 12: The diagram of MSE changing with tap-length.

The algorithm presented in this paper has two stages, EEMD-PR and LMS, respectively, EEMD-PR provides effects of reference signal training, and LMS fulfils denoising process online. In the comparisons, the EEMD-PR and LMS used in this paper are compared with related algorithms, respectively. According to Figure 14 and Table 1, the algorithm of this paper has higher accuracy, and the trend of signal variation and details can be retained in the results effectively. EEMD-IT and wavelet thresholding can retain the trend of signal variation but useful details are neglected. However, EEMD-PR cannot distinguish useful details and noise, and effectiveness is depressed severely.

According to [35], n_m IMFs are extracted from signal with length n, where $n_m \leq \log_2^n$, the space complexities of EMD-PR (with pdf), EMD-IT (with pdf) are approximate $[(13 + n_m)n + 100n_m + n]$ and $[(13 + n_m)n + 100n_m + 100n_m]$, respectively, due to EEMD is applied in this paper, and ensemble number is 200, and in this condition, the EEMD-PR (with pdf) and EEMD-IT (with pdf) are [200 $(13 + n_m)n + 100n_m + n$] and [200 $(13 + n_m)n + 100n_m + 100n_m$]. EMD consumes considerable amount of storage resources, although EEMD can improve accuracy, incremental consumptions of storage are inevitable.
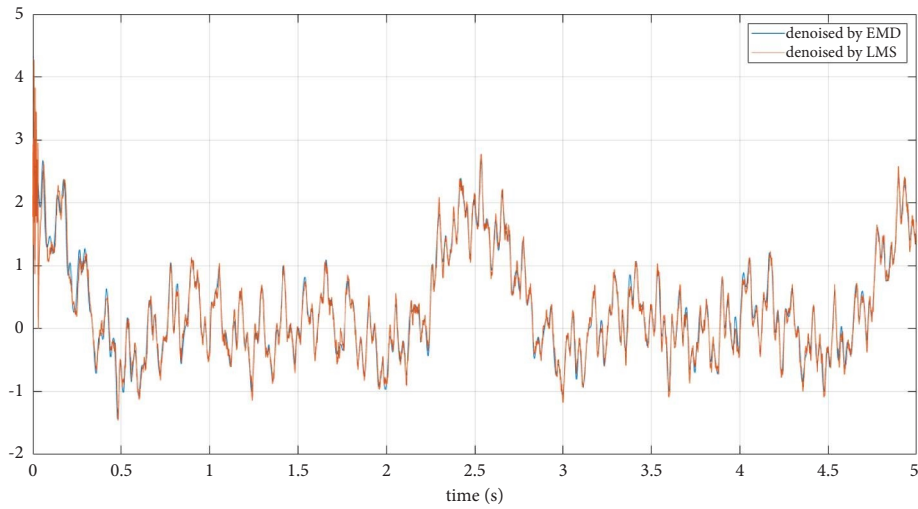
Figure 13: The diagram of LMS filter result.

(a)

(b)

(c)
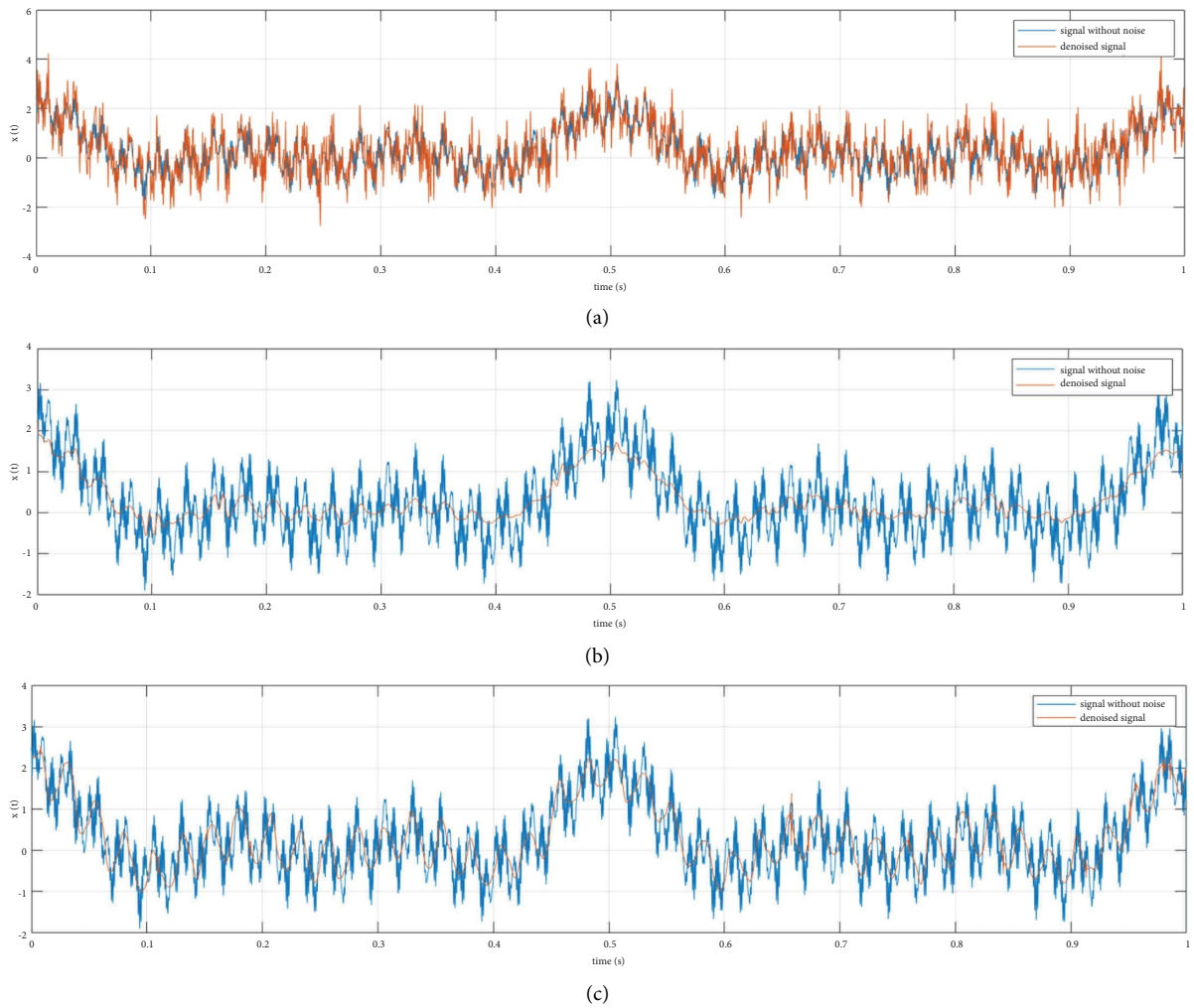
Figure 14: Denoising results with related algorithms. (a) Denoising results with EEMD-PR and sample entropy. (b) Denoising results with EEMD-IT. (c) Denoising results with wavelet thresholding.

TABLE 1: The accuracy comparisons of related algorithms.

	EEMD-PR in this paper	LMS in this paper	EEMD-PR with sample entropy	EEMD-IT	Wavelet
SNR	6.49	5.72	5.77	−5.22	4.61
RMSE	0.4454	0.4804	0.5166	0.5398	0.4571
MAE	0.3625	0.3912	0.4104	0.4367	0.3786

TABLE 2: The time cost comparisons of related algorithms.

	EEMD-PR in this paper	LMS in this paper	EEMD-PR with sample entropy	EEMD-IT	Wavelet
Time cost(s)	35.1606	0.0815	32.7806	34.1204	0.7829

Time consumptions of EEMD-PR in this paper, EEMD-PR with sample entropy, EEMD-IT are comparable, primarily due to the dominant time consumption of EEMD. For the long processing time, these 3 algorithms are not suitable for the online applications. This paper EEMD-PR is used for acquisition of reference signal beforehand; storage and time consumptions will not affect practical application. LMS has quick enough response and less storage spaces; therefore, the algorithm presented in this paper is able to satisfy application requirements.

5. The Application in Precise Mechanical Transmission

RV reducer is a widely used precise transmission mechanism, which is combined with cycloid-pin reducer and planetary reducer. In engineering application, the control system depends on the measuring facilities to achieve the control accuracy, even the reducer has good kinematic quality, and the sufficient precise measuring data are still a critical factor to fulfill the ideal performance for the whole system. The presented approach is applied in the RV reducer motion parameters denoising to acquire the more accurate data. The experiments are conducted on a dedicated measurement platform.

5.1. The Experiment Facilities and Results. Usually, the measurement results of transmission motion are used directly for control and monitoring. In actual working condition, however, measurement results include non-negligible noise, the signal including noise will lead to the extra error, unsmooth output; in extreme situation, it can lead to system instability. Under the requirement of precise transmission, it is necessary to process the output motion parameter and acquire more precise and smooth data.

For the purposes mentioned above, the measurement facilities of precision reducer motion are developed, as shown in Figure 15, and experiments are carried out. The model of reducer is RV-40E, and its transmission ratio is 121, due to the large difference between input and output, the Kistler 4502A and 4503A are used respectively to measure
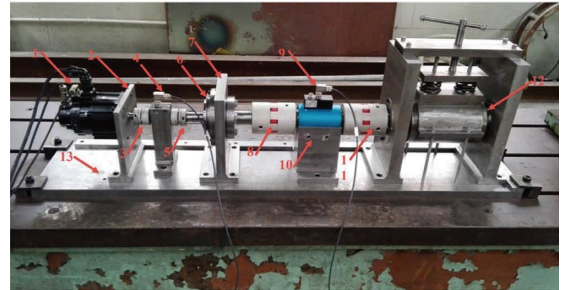
FIGURE 15: Picture of facilities for precision reducer motion. (1) Motor, (2) motor plate, (3) input coupler I, (4) input sensor, (5) input coupler II, (6) RV reducer, (7) reducer plate, (8) output coupler I, (9) output sensor, (10) senor platform, (11) output coupler II, (12) load mechanism, and (13) bottom plate.

the velocity and torque. The test conditions are separated at 1000 r/min, 2000 r/min, and 3000 r/min, and the instantaneous rotation speed and torque are collected; the sample frequency is 1 kHz.

The experiment data at different conditions are shown in Figure 16; the coefficient of variation is all narrow in the rotation speed of input and output; this indicates that the rotation speed is stable in the reducer operation, and noise components can be ignored.

However, in all three conditions, there are tremendous changes of torque in the operation process, and the coefficient of variation of torque is much larger than the rotation speed. It can be concluded that the noise components cannot be ignored, and it is necessary to wipe off the noise composition.

5.2. The Denoising of Torque Signals. The input torque and the output at 3 items of condition are decomposed by EMD and the results are shown in Figure 17.

The CMSE calculation is shown in Figure 18, and the PDF of IMF and original signals are shown in Figure 19; the $\ell 2$-norm of torque is shown in Figure 20. No matter which rotation speed, the CMSE of the last stage IMF is obviously larger than other CMSE of the initial stages of IMF, which means the information components are dominant in the last stage signal and coincides the situation in which operation
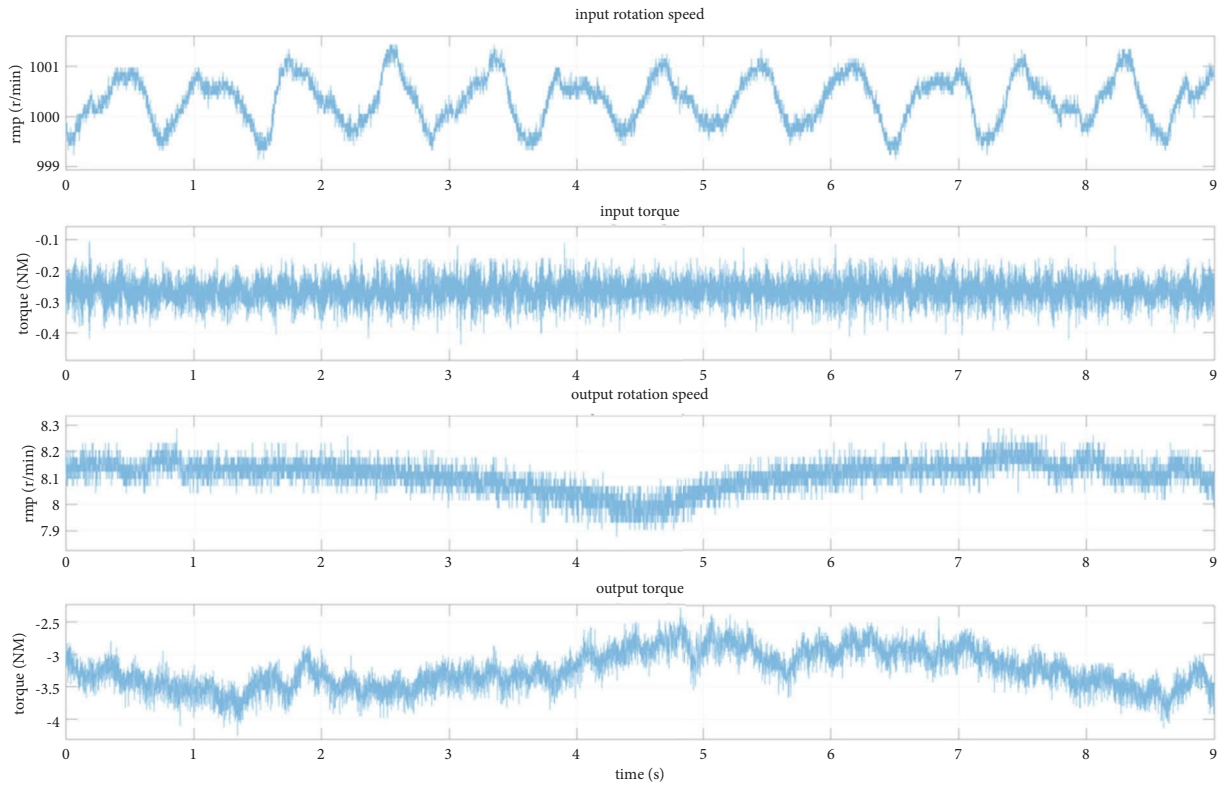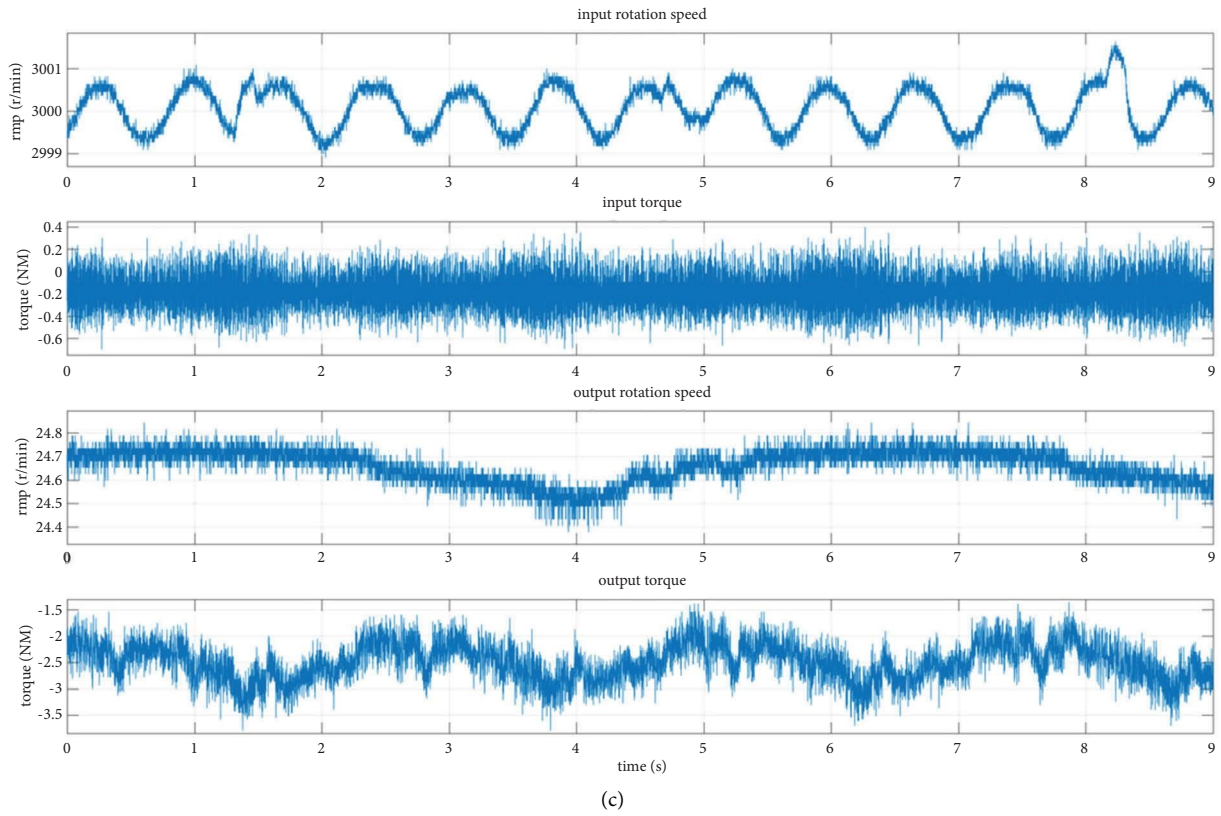
(a)
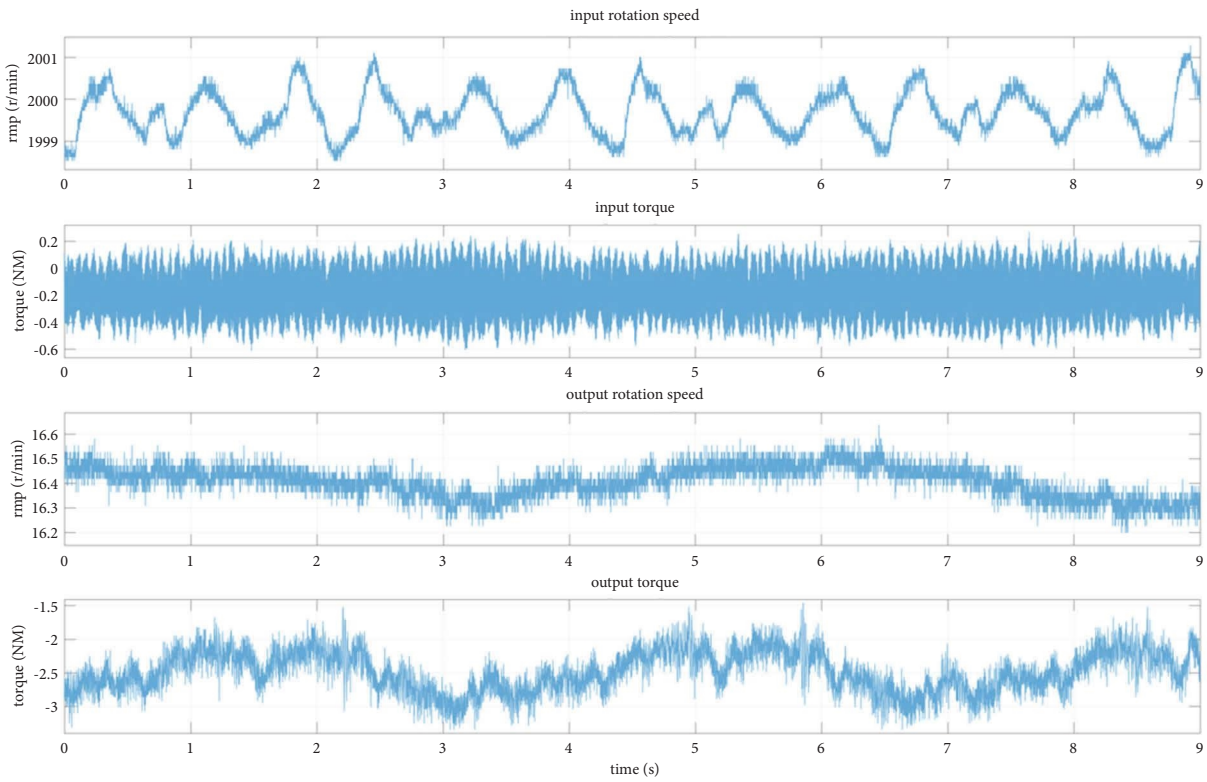
(b)

FIGURE 16: Continued.

(c)

Figure 16: The experiment data of motion parameter under different conditions. (a) Measuring motion parameters data at 1000 r/min. (b) Measuring motion parameters data at 2000 r/min. (c) Measuring motion parameters data at 3000 r/min.
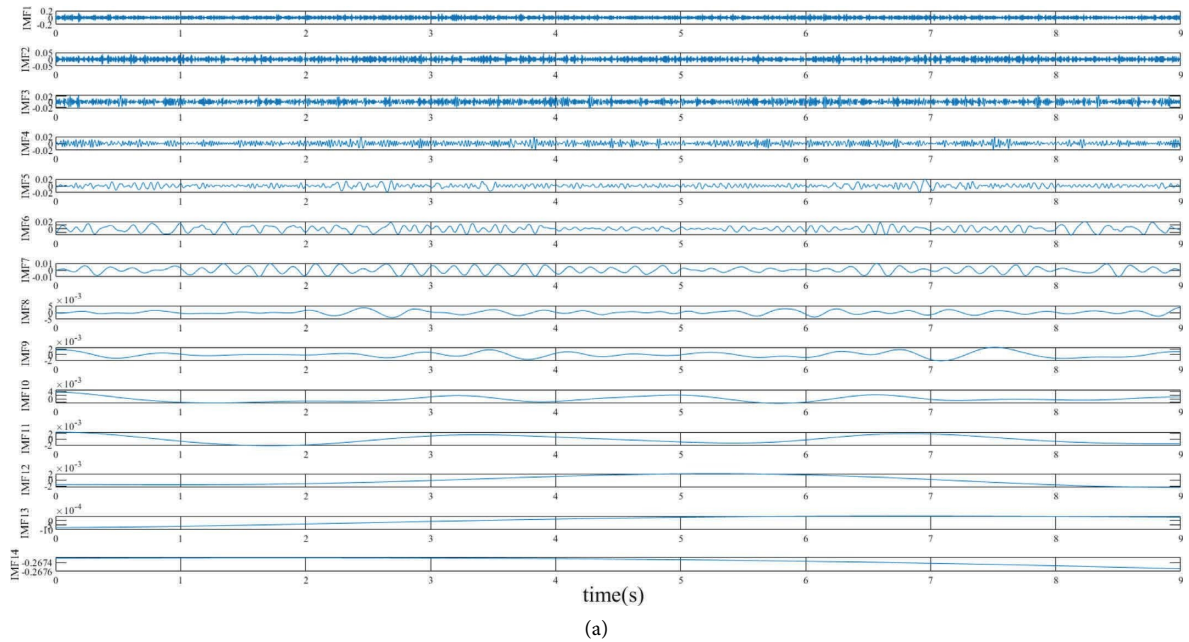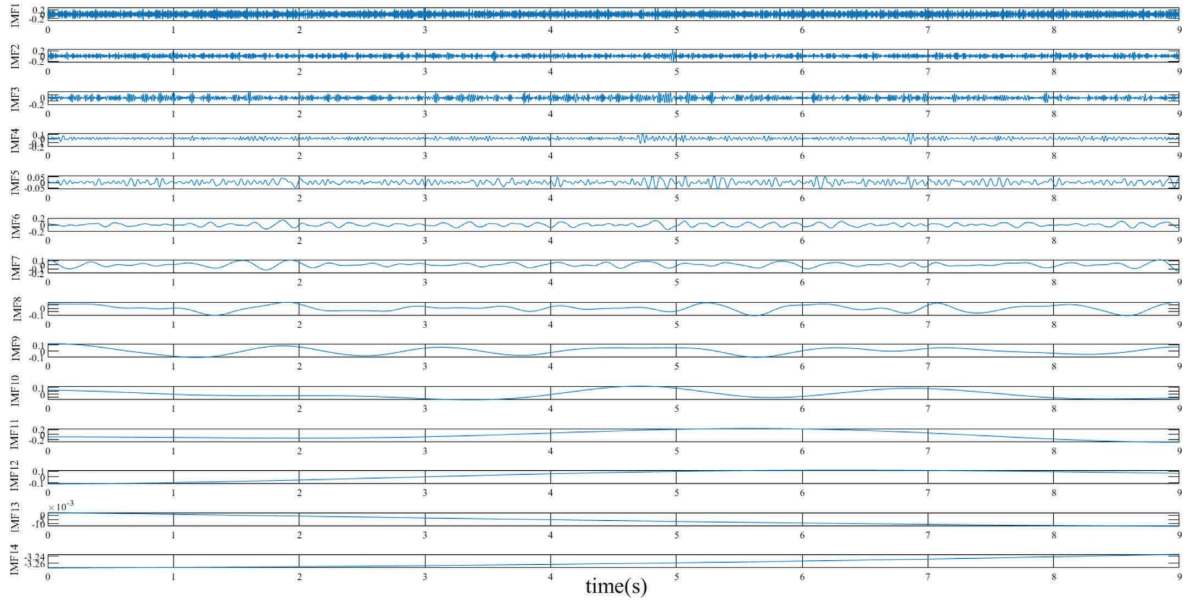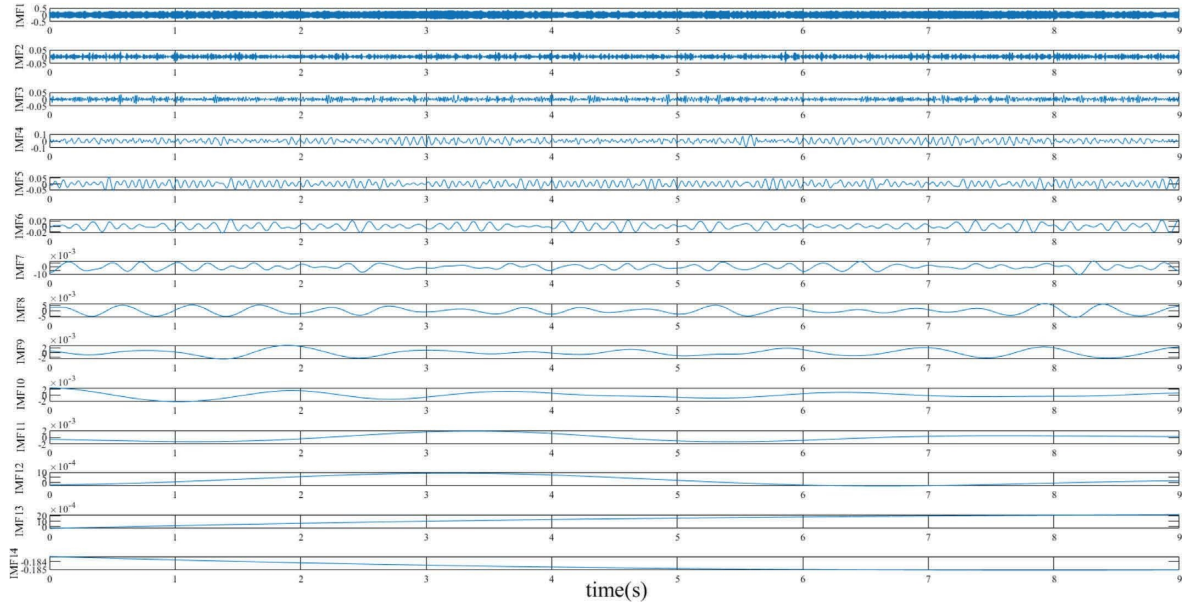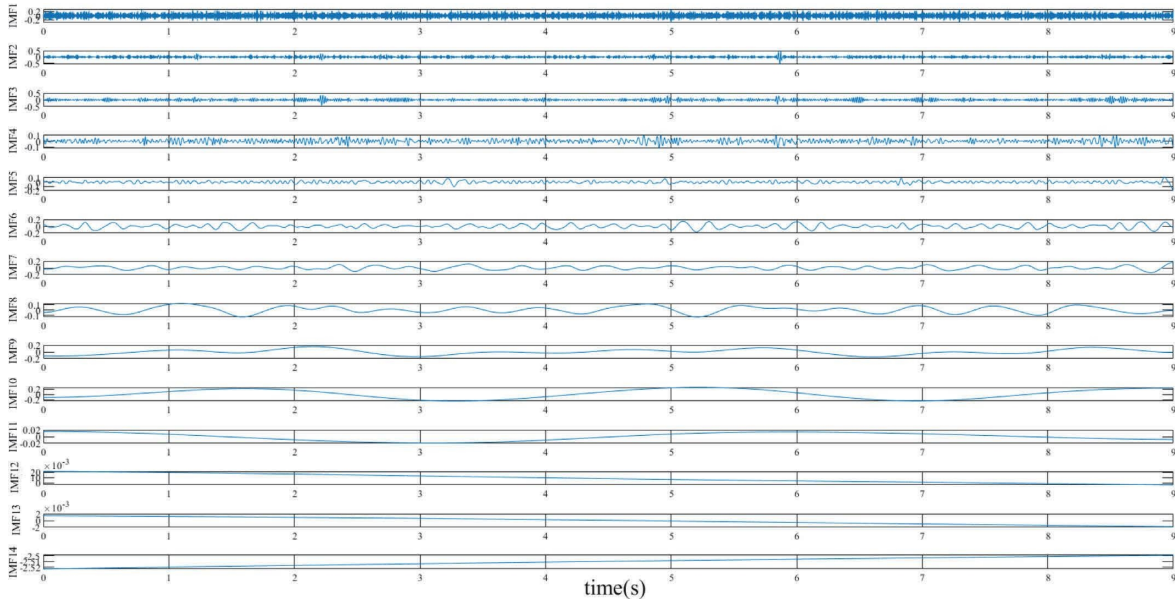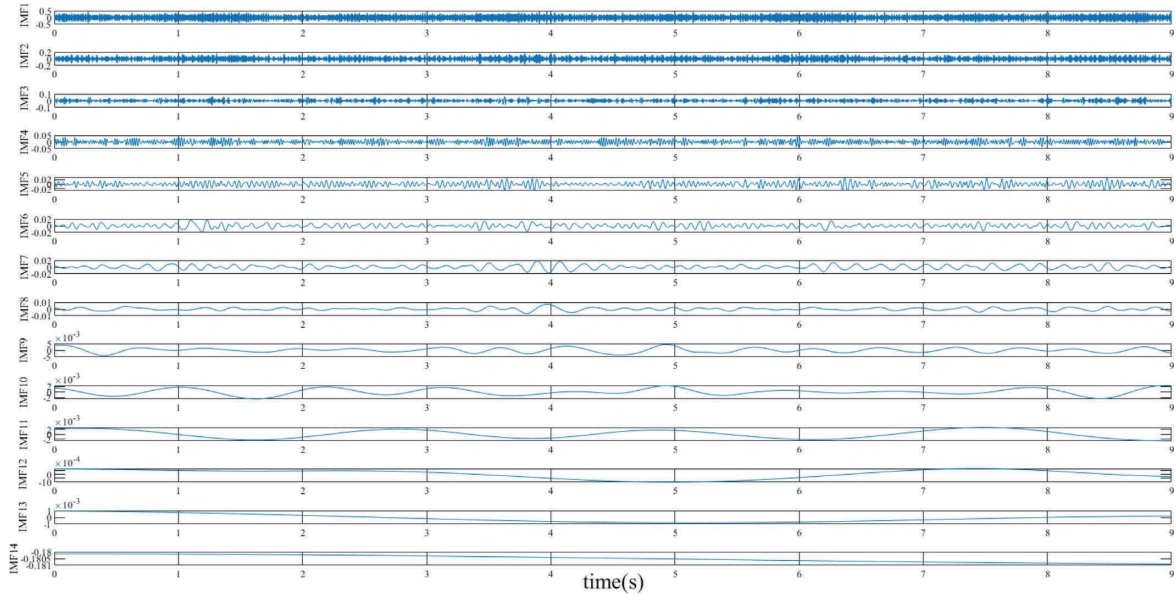

(a)

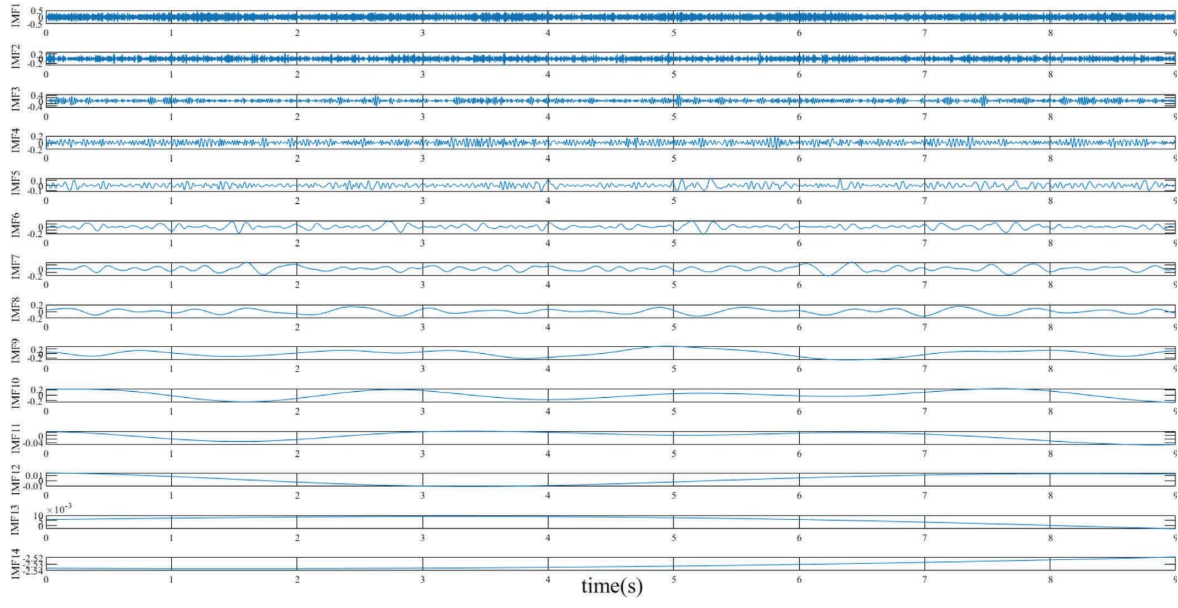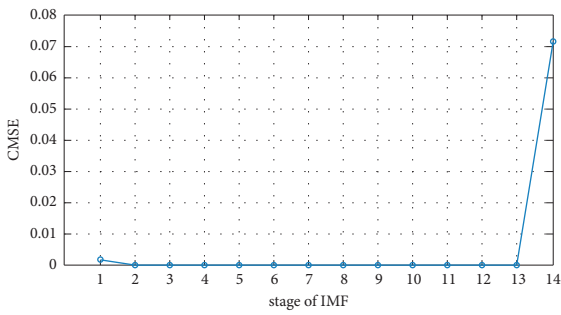Figure 17: Continued.

(b)


(c)

Figure 17: Continued.

(d)

(e)

Figure 17: Continued.

(f)

FIGURE 17: EMD results of torque at different rotation speeds. (a) The EMD results of input torque at 1000 r/min. (b) The EMD results of output torque at 1000 r/min. (c) The EMD results of input torque at 2000 r/min. (d) The EMD results of output torque at 2000 r/min. (e) The EMD results of input torque at 3000 r/min. (f) The EMD results of output torque at 3000 r/min.

(a)
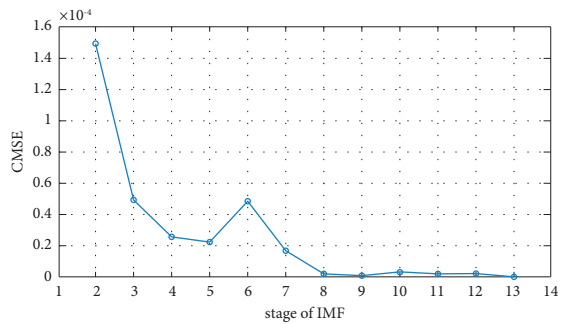
(b)
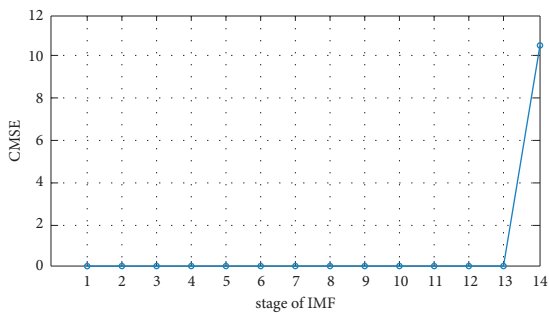
(c)
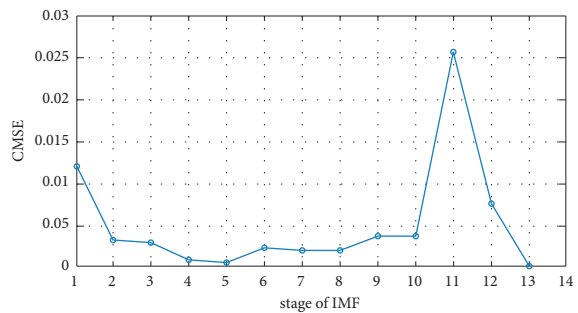
(d)

FIGURE 18: Continued.
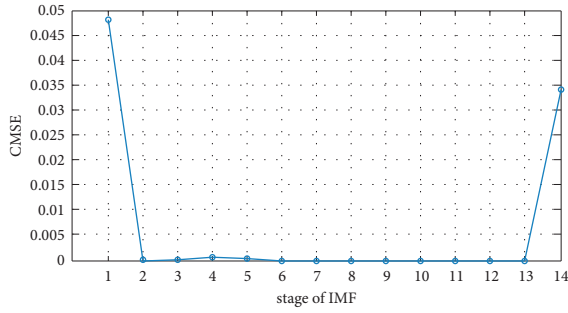
(e)
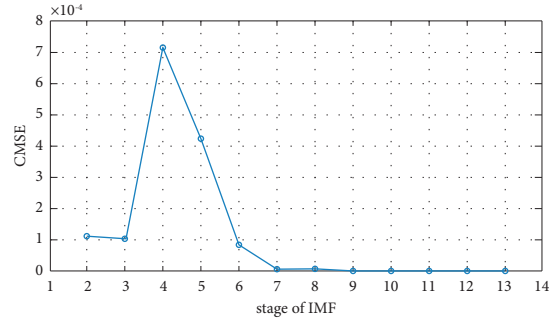
(f)
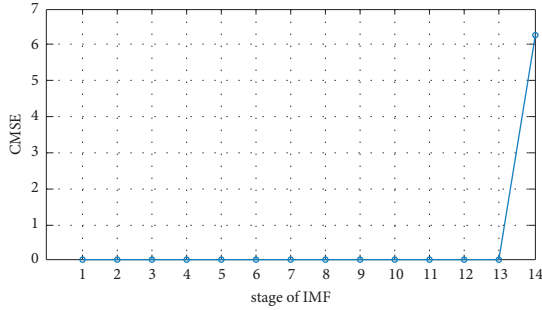
(g)
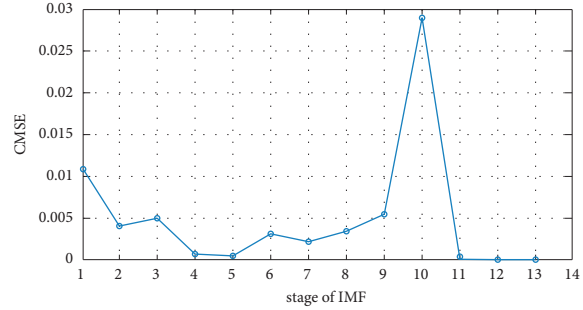
(h)
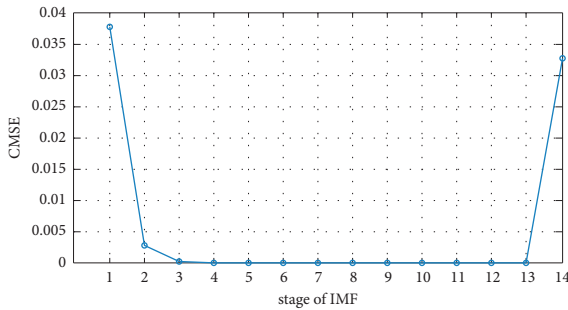
(i)
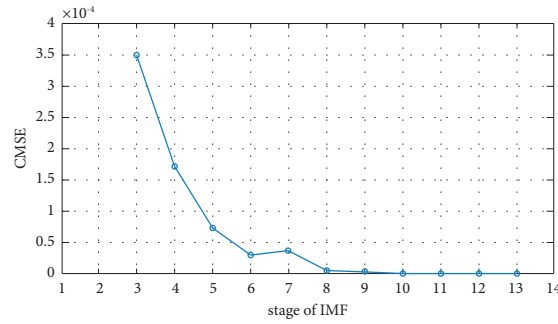
(j)
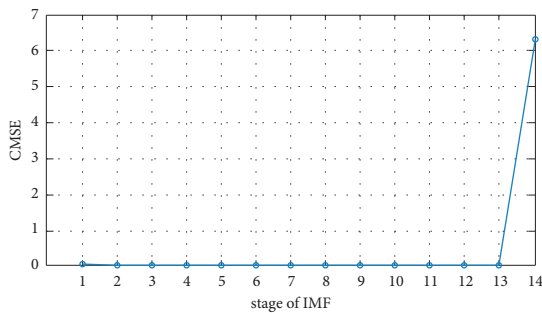
(k)
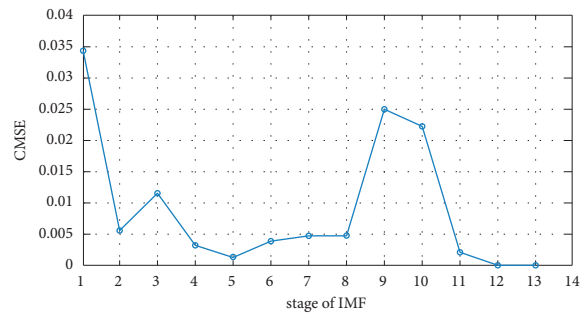
(l)

Figure 18: The diagram of CMSE index of torque. (a) CMSE of input torque IMF at 1000 r/min. (b) Part of CMSE of input torque IMF at 1000 r/min. (c) CMSE of output torque IMF at 1000 r/min. (d) Part of CMSE of output torque IMF at 1000 r/min. (e) CMSE of input torque IMF at 2000 r/min. (f) Part of CMSE of input torque IMF at 2000 r/min. (g) CMSE of output torque IMF at 2000 r/min. (h) Part of CMSE of output torque IMF at 2000 r/min. (i) CMSE of input torque IMF at 3000 r/min. (j) Part of CMSE of input torque IMF at 3000 r/min. (k) CMSE of output torque IMF at 3000 r/min. (l) Part of CMSE of output torque IMF at 3000 r/min.
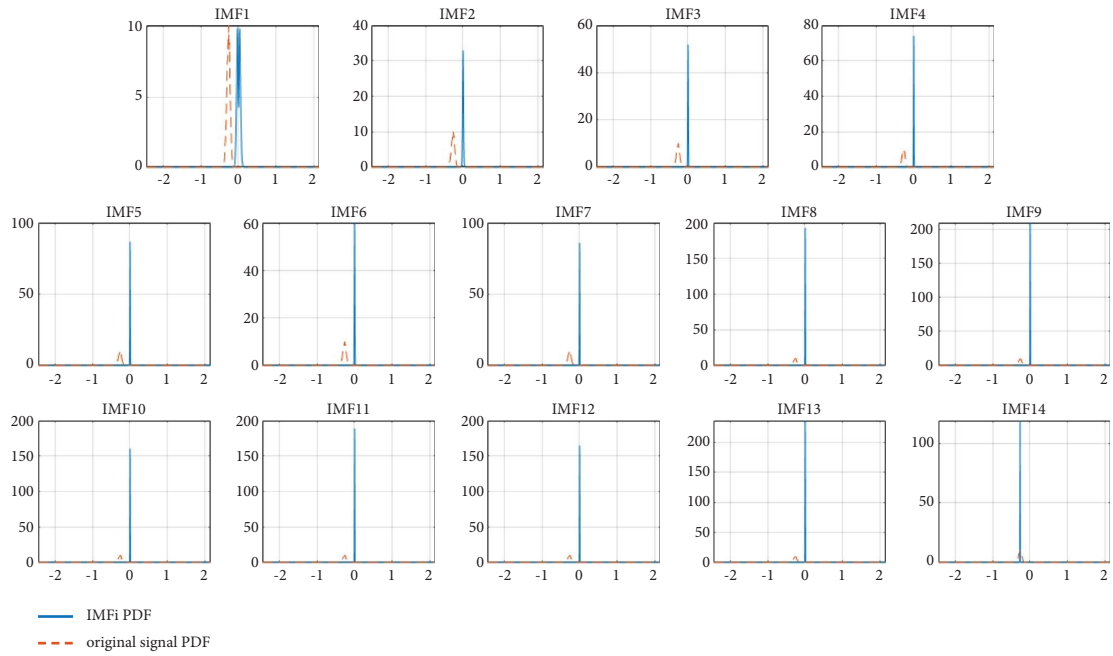
(a)
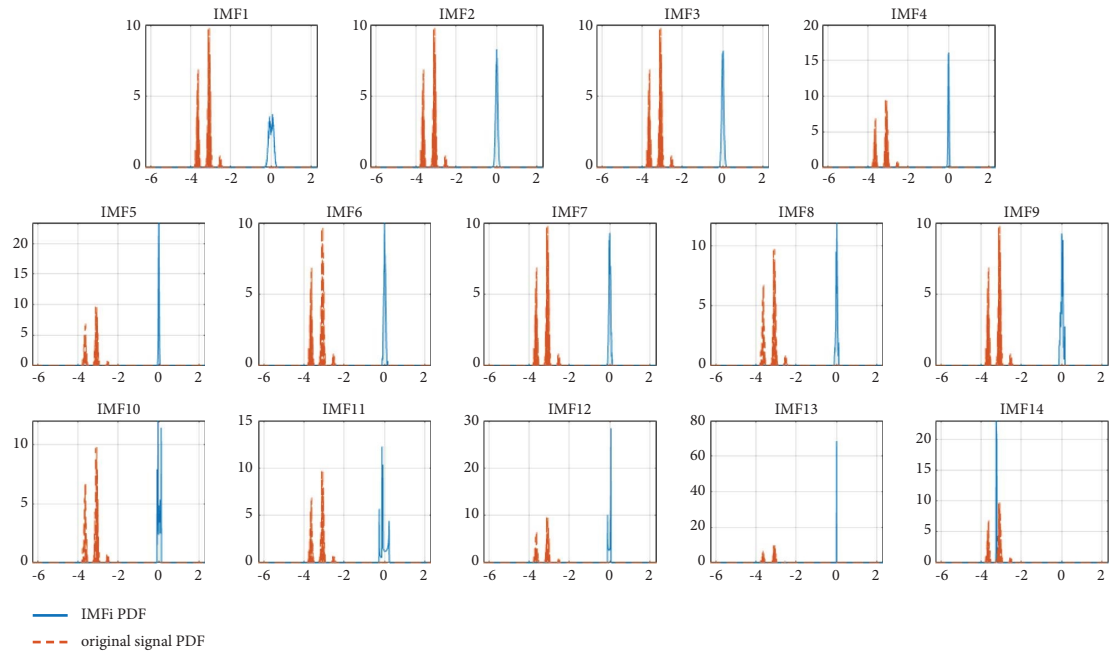
(b)

Figure 19: Continued.
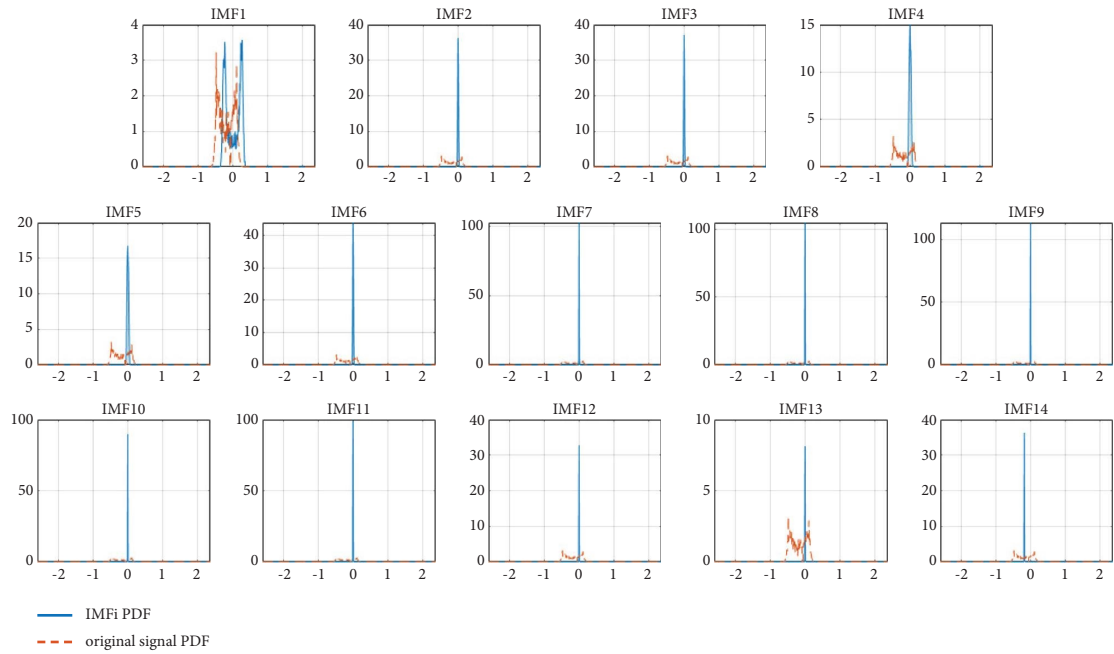
(c)
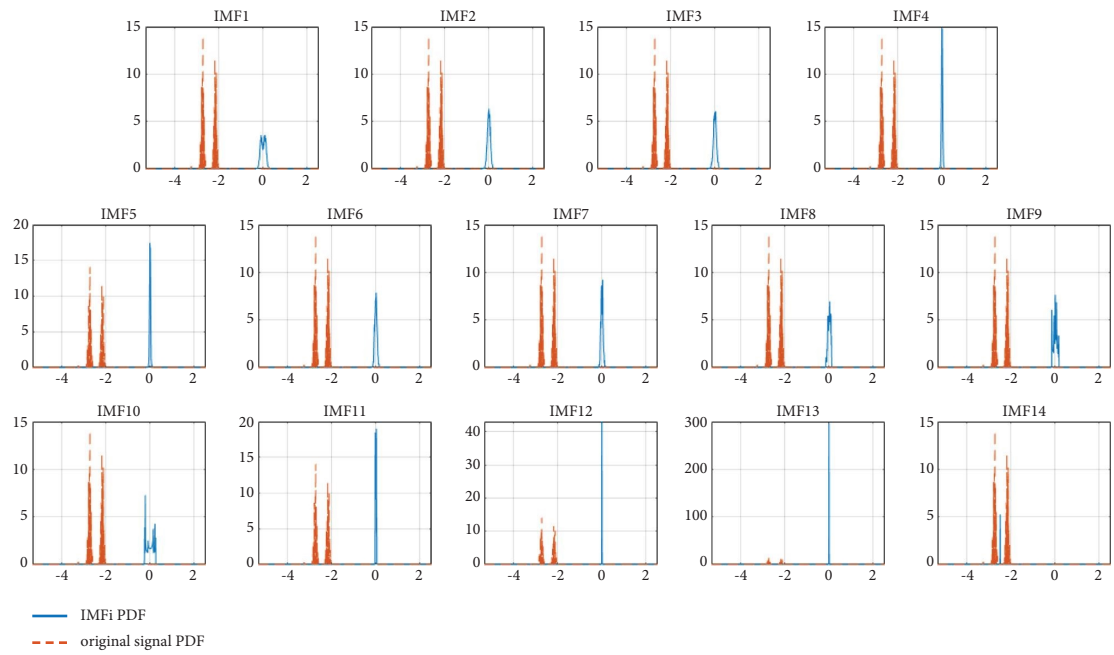
(d)

Figure 19: Continued.
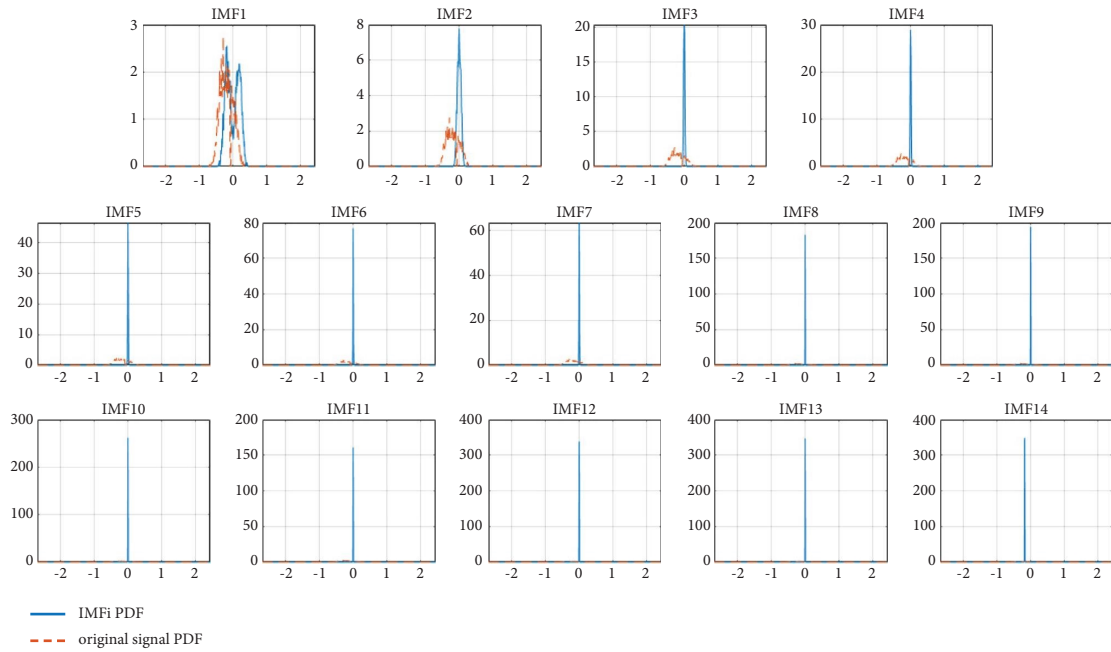
(e)
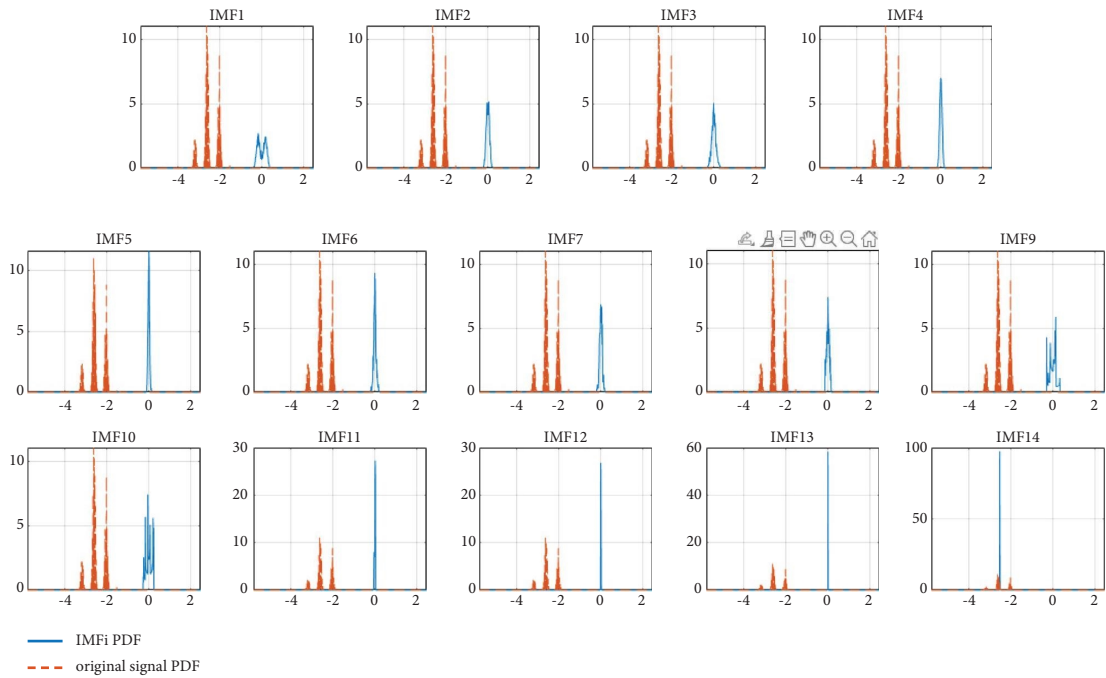
(f)

Figure 19: The diagram of PDF of original torque signal and IMF. (a) The PDF of original signal and IMF at 1000 r/min input torque. (b) The PDF of original signal and IMF at 1000 r/min output torque. (c) The PDF of original signal and IMF at 2000 r/min input torque. (d) The PDF of origi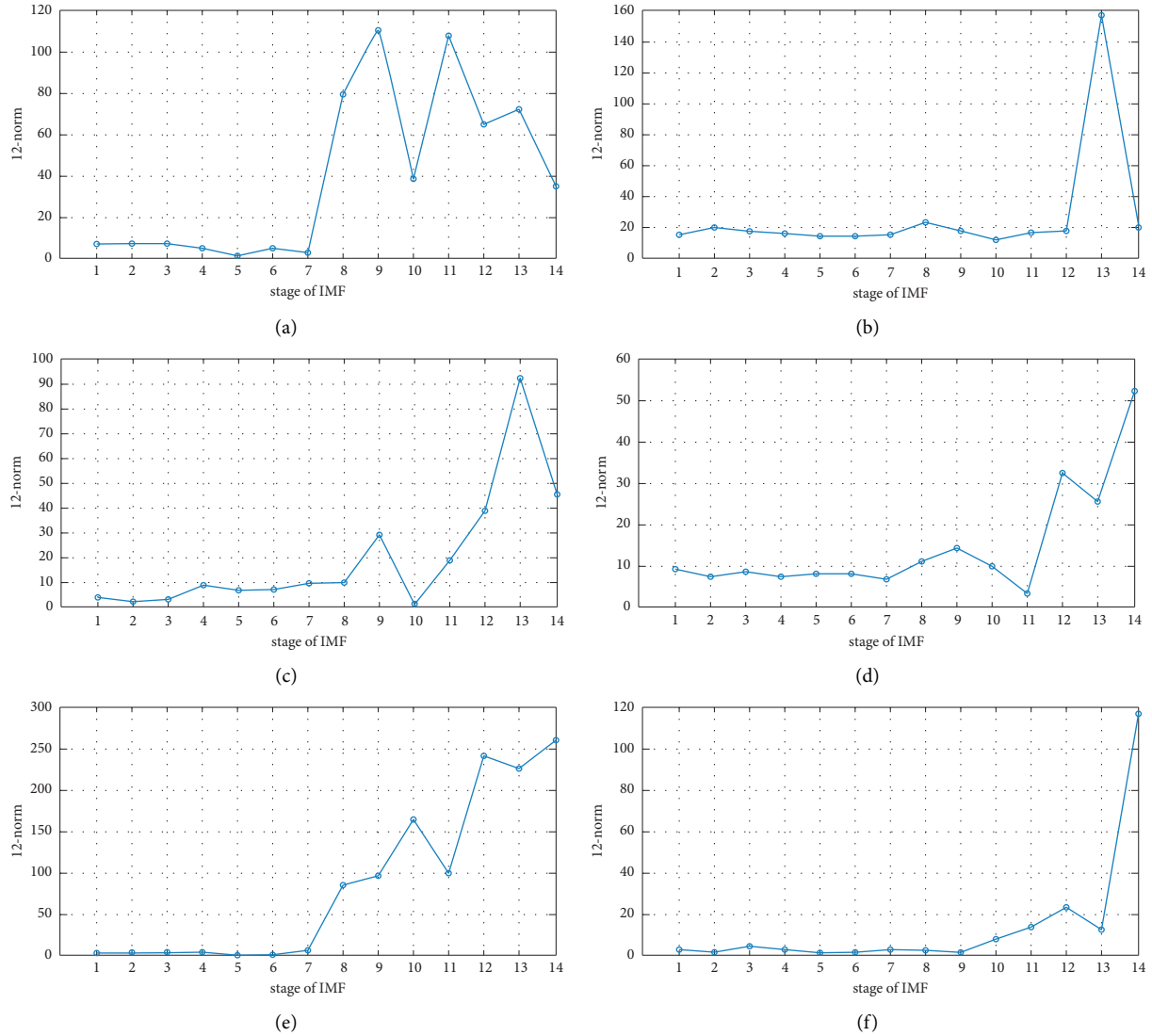nal signal and IMF at 2000 r/min output torque. (e) The PDF of original signal and IMF at 3000 r/min input torque. (f) The PDF of original signal and IMF at 3000 r/min output torque.

Figure 20: The diagram of $\ell 2$-norm of simulation signal. (a) $\ell 2$-norm of input torque at 1000 r/min. (b) $\ell 2$-norm of output torque at 1000 r/min. (c) $\ell 2$-norm of input torque at 2000 r/min. (d) $\ell 2$-norm of output torque at 2000 r/min. (e) $\ell 2$-norm of input torque at 3000 r/min. (f) $\ell 2$-norm of output torque at 3000 r/min.

Table 3: The stage numbers of 3 torque signal parts.

	Input torque at 1000 r/min	Output torque at 1000 r/min	Input torque at 2000 r/min	Output torque at 2000 r/min	Input torque at 3000 r/min	Output torque at 3000 r/min
Noise components	1–5	1–5	1–3	1–2	1–6	1–2
Mixed components	6–9	6–8	4–9	3–9	7–10	3–5
Information components	10–14	9–14	10–14	10–14	11–14	6–14

load is stable. There is one peak in the PDF of input torque, there are multiple peaks in the PDF of output torque, and it can infer that the reducer brings extra disturbance and will affect the stability of operation. The respective shapes of IMF PDFs are concentrated; it indicates the EMD algorithm can effectively extract monotonous component from the torque signal. The $\ell 2$-norm of upper stages of IMFs is much larger than the lower stages of IMFs that the upper stages are dominated by information. For the torque denoising, the information components mainly locate in specific stage, and the band of stage related with information components is narrow.

According to the calculation results of CMSE and $\ell 2$-norm, IMFs of torque can be separated noise components, mixed components, and information components, the consequences are shown in Table 3.
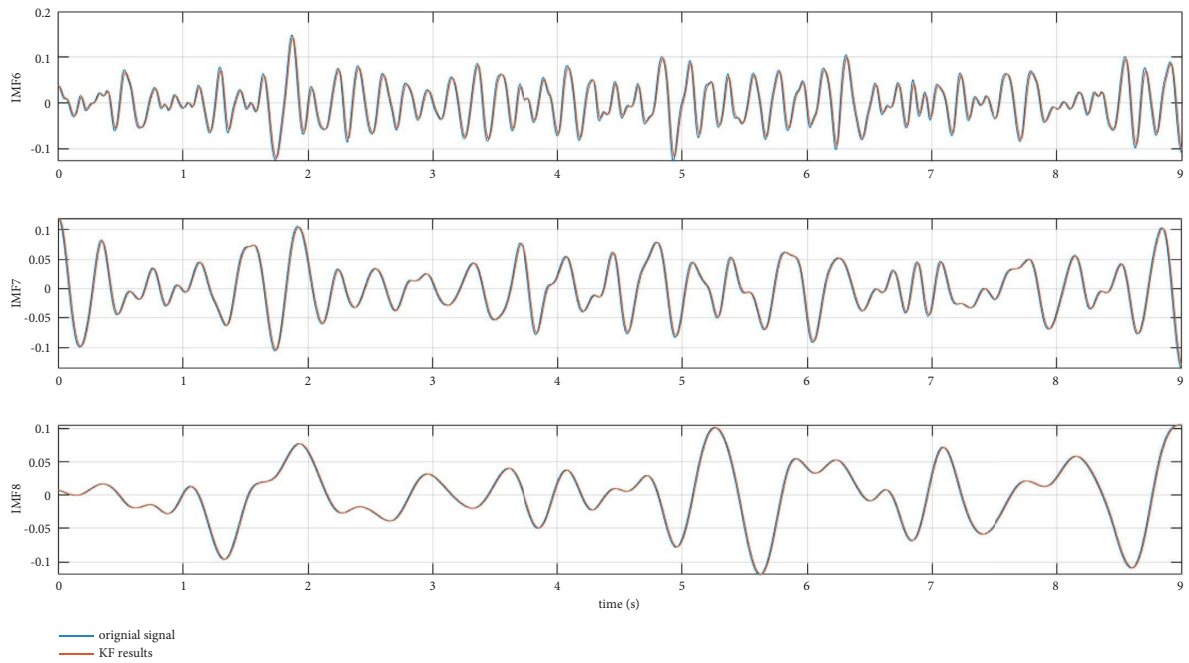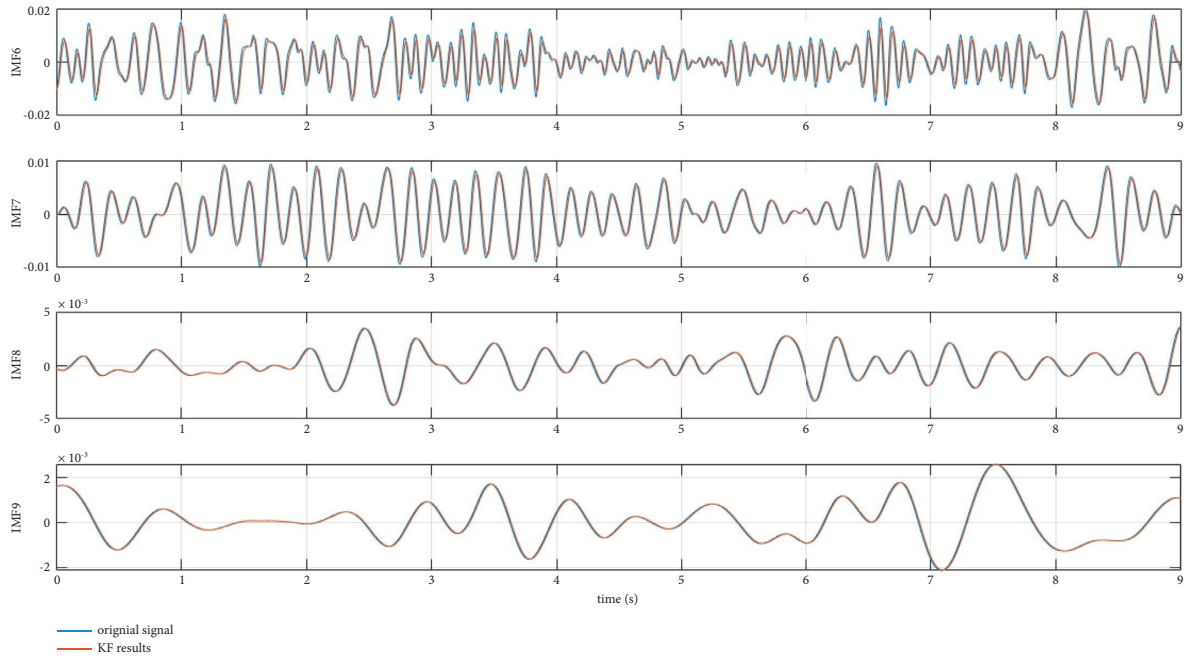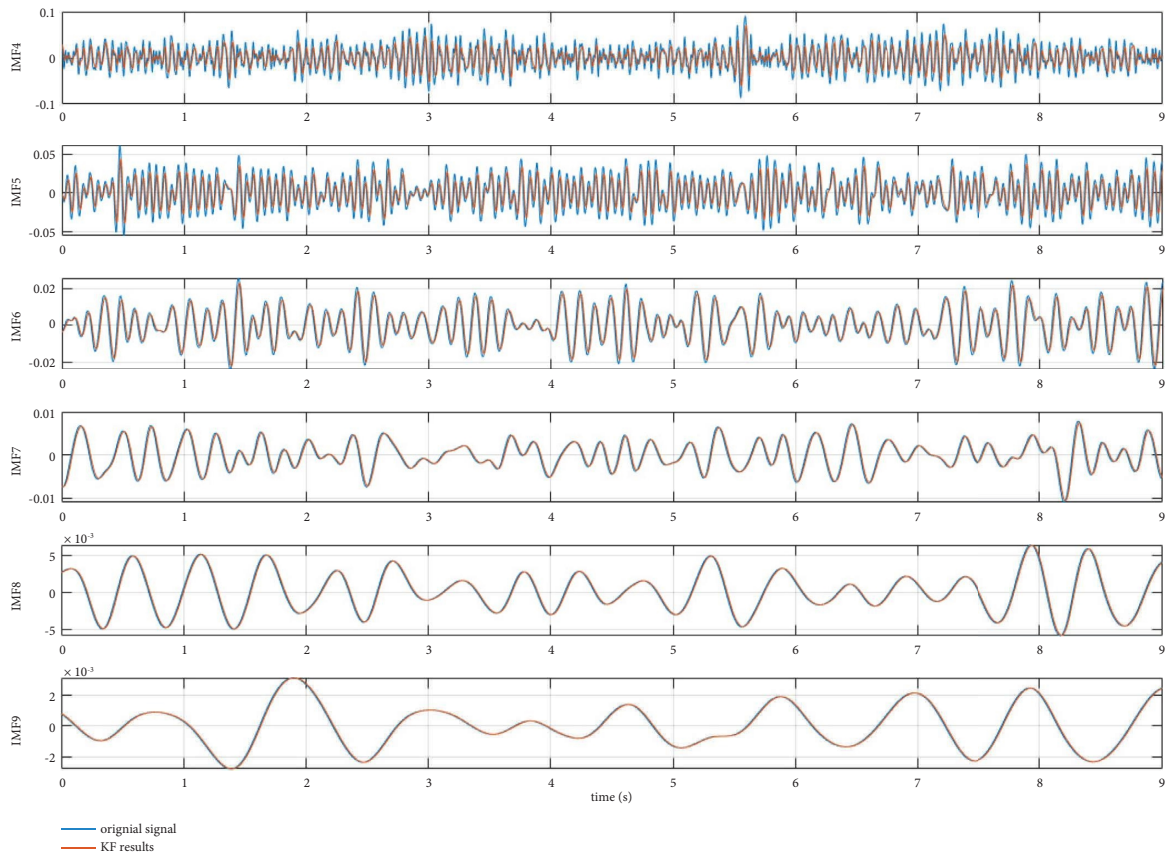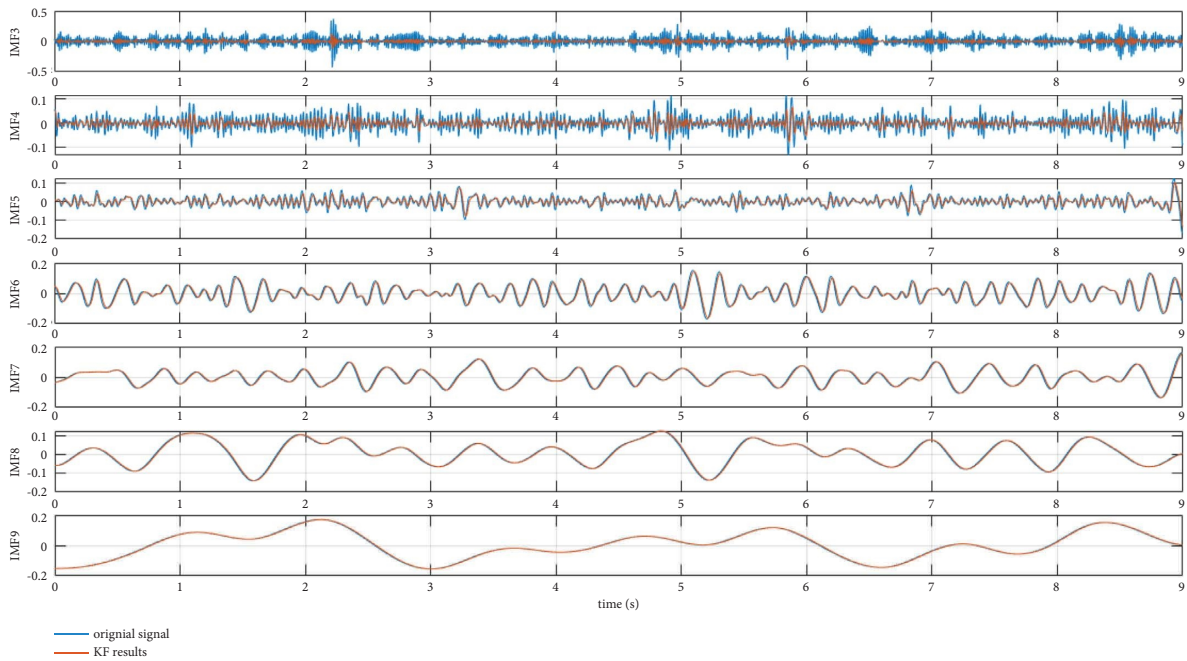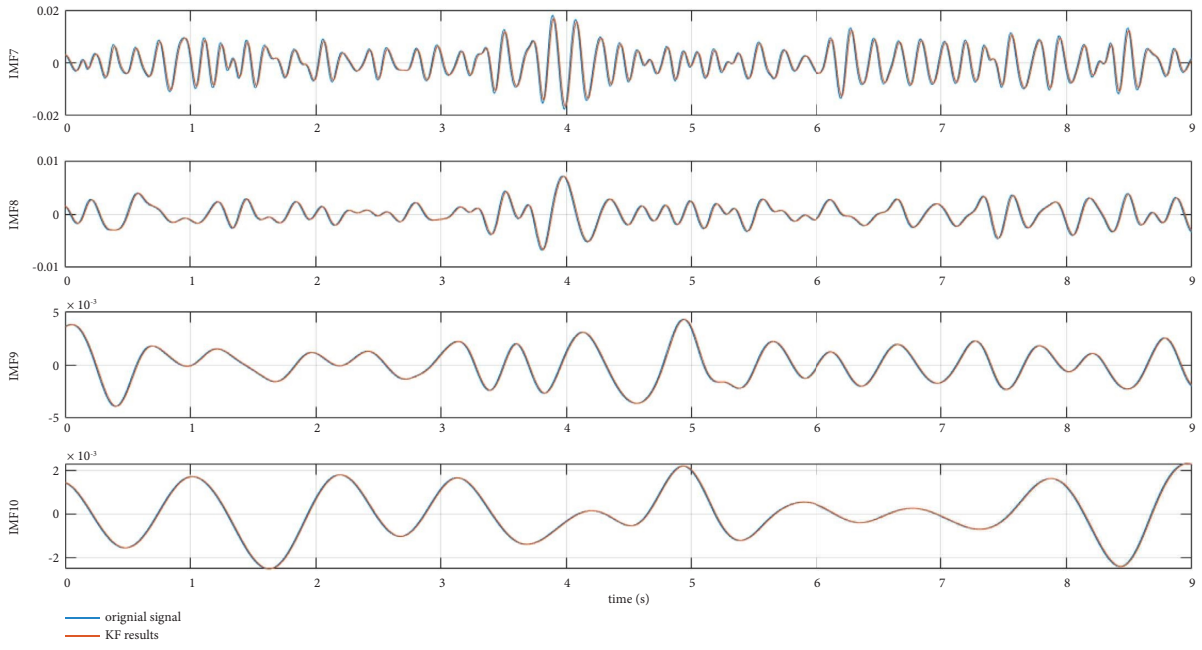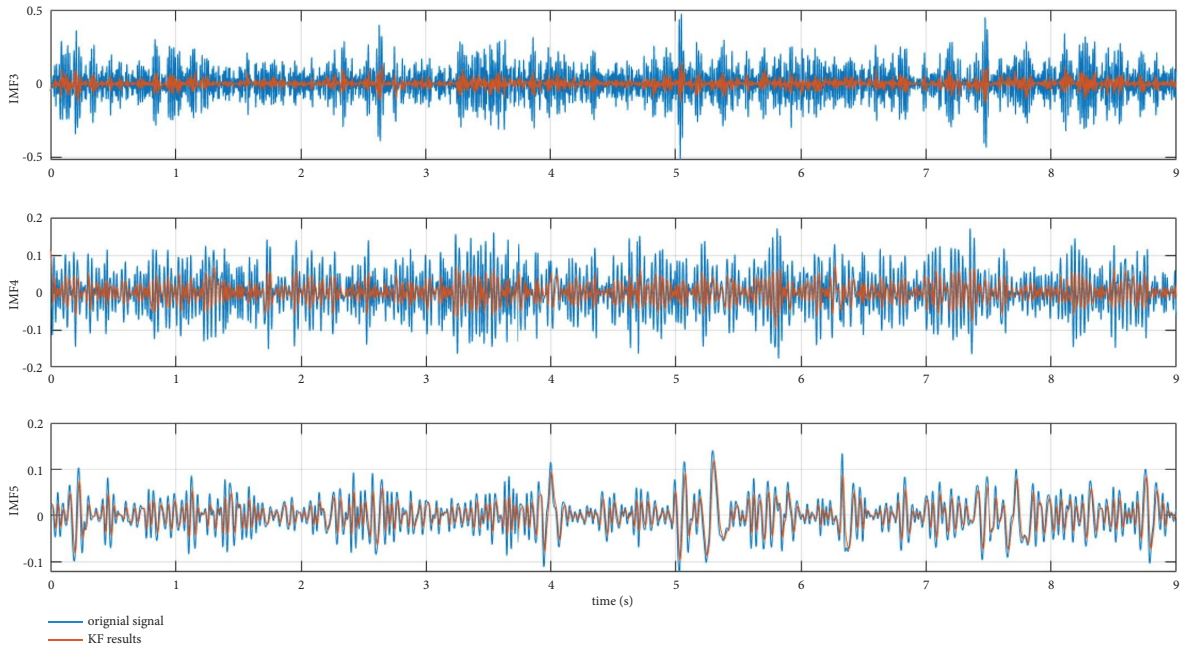
(a)

(b)

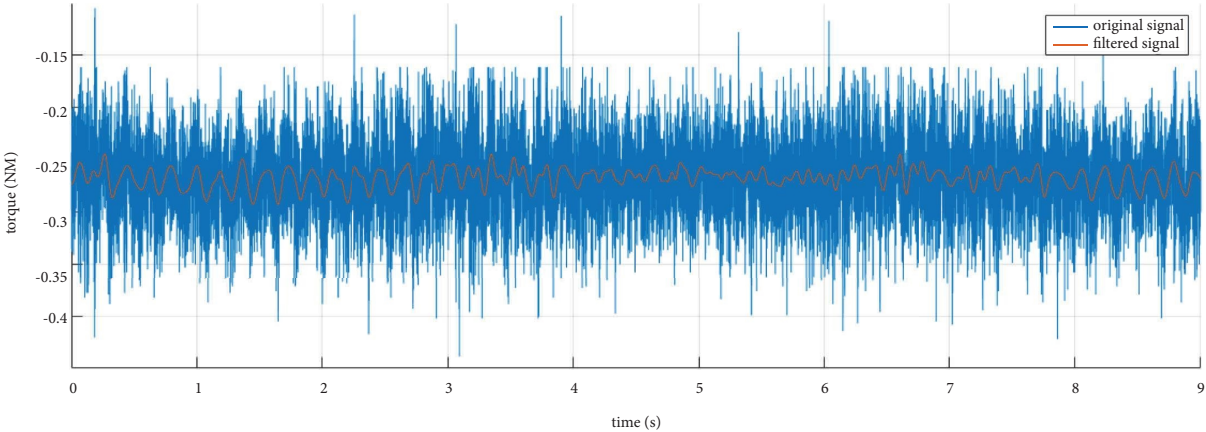Figure 21: Continued.

(c)

(d)

Figure 21: Continued.

(e)

(f)

FIGURE 21: Kalman filter results for mixed components. (a) Kalman filter results for mixed components of input torque at 1000 r/min. (b) Kalman filter results for mixed components of output torque at 1000 r/min. (c) Kalman filter results for mixed components of input torque at 2000 r/min. (d) Kalman filter results for mixed components of output torque at 2000 r/min. (e) Kalman filter results for mixed components of input torque at 3000 r/min. (f) Kalman filter results for mixed components of output torque at 3000 r/min.
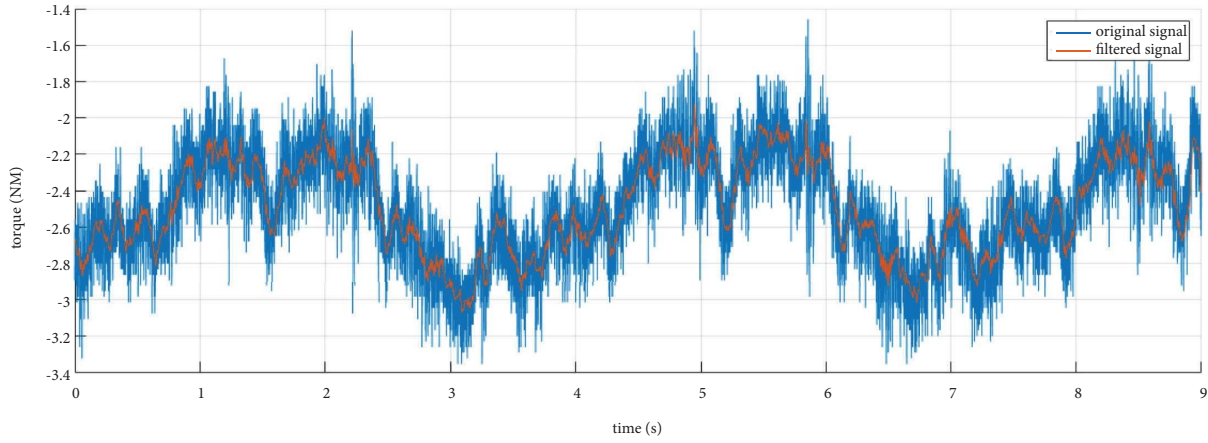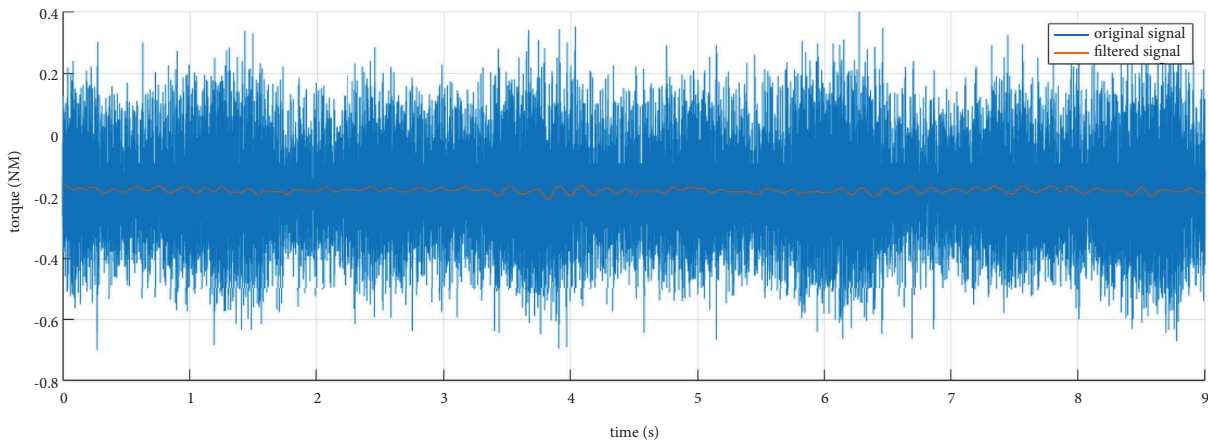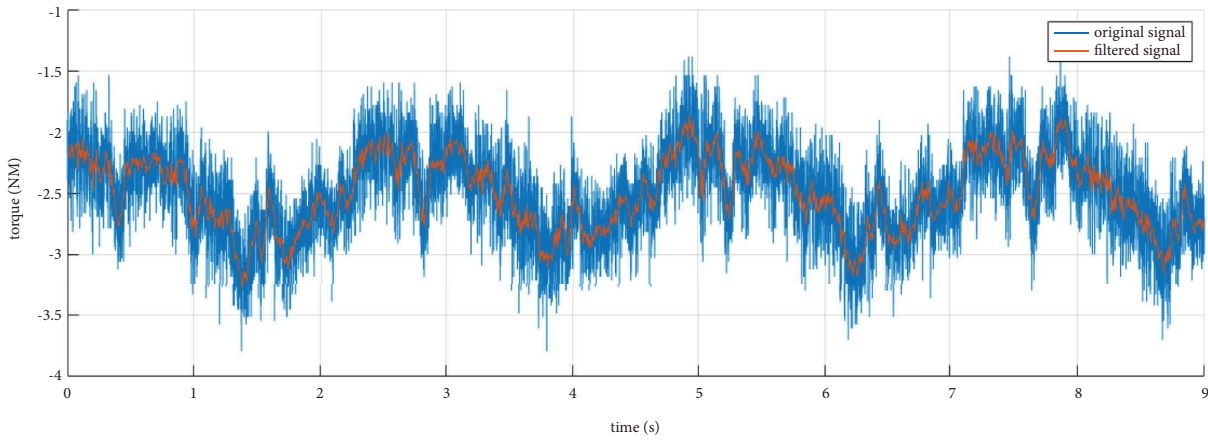
(a)
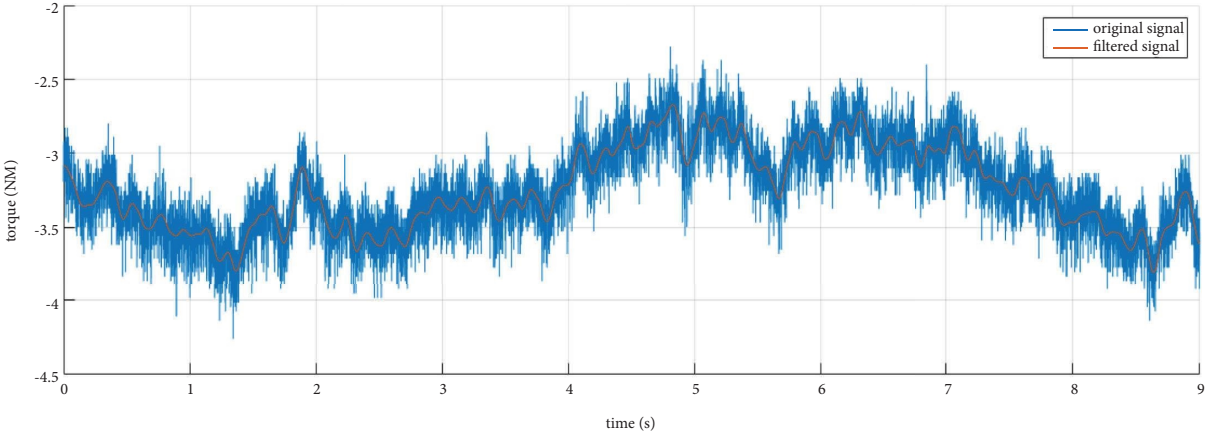

(b)
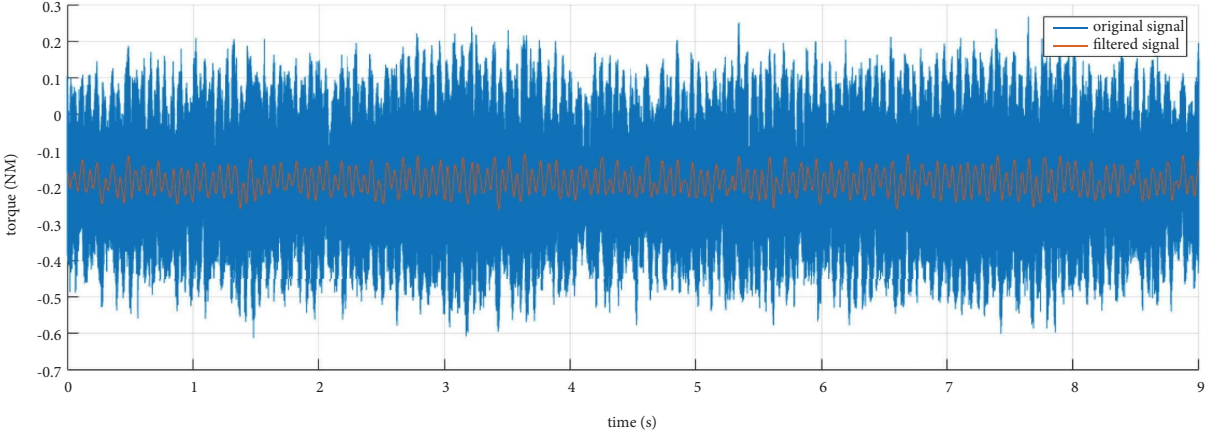
(c)

Figure 22: Continued.

(d)

(e)

(f)

FIGURE 22: The diagram of denoised torque. (a) The denoised input torque signal at 1000 r/min. (b) The denoised output torque signal at 1000 r/min. (c) The denoised input torque signal at 2000 r/min. (d) The denoised output torque signal at 2000 r/min. (e) The denoised input torque signal at 3000 r/min. (f) The denoised output torque signal at 3000 r/min.

TABLE 4: SNR comparison between original and denoised signals.

	Input torque at 1000 r/min	Output torque at 1000 r/min	Input torque at 2000 r/min	Output torque at 2000 r/min	Input torque at 3000 r/min	Output torque at 3000 r/min
Original signal SNR	15.68	25.80	−1.37	23.68	−0.48	19.69
Denoised signal SNR	29.64	31.44	25.18	40.32	27.30	28.90
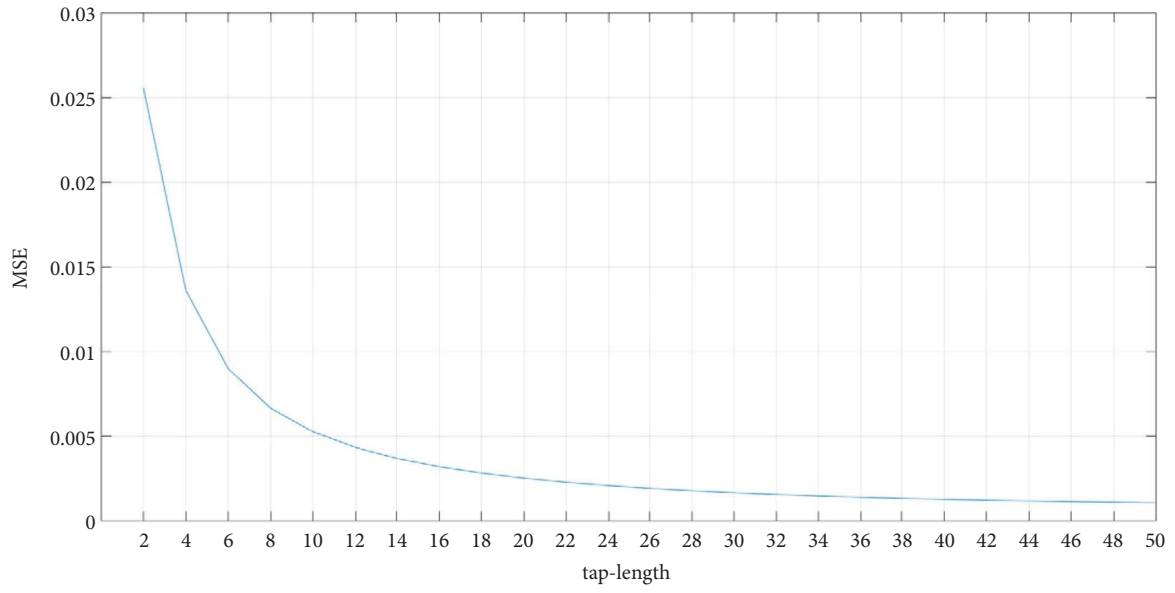
(a)
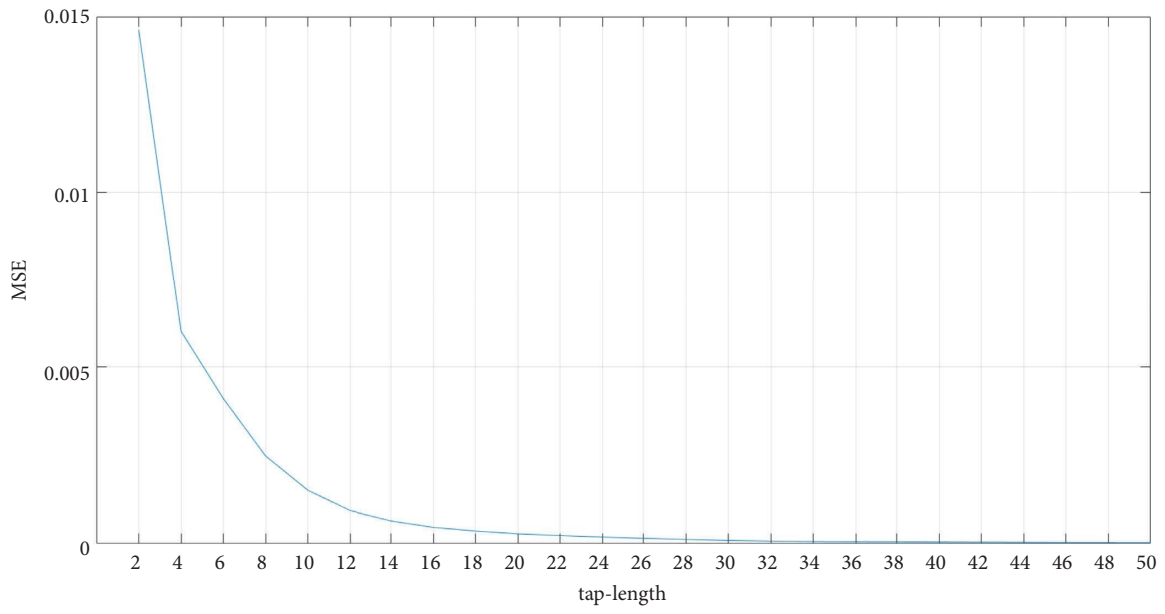
(b)

Figure 23: Continued.
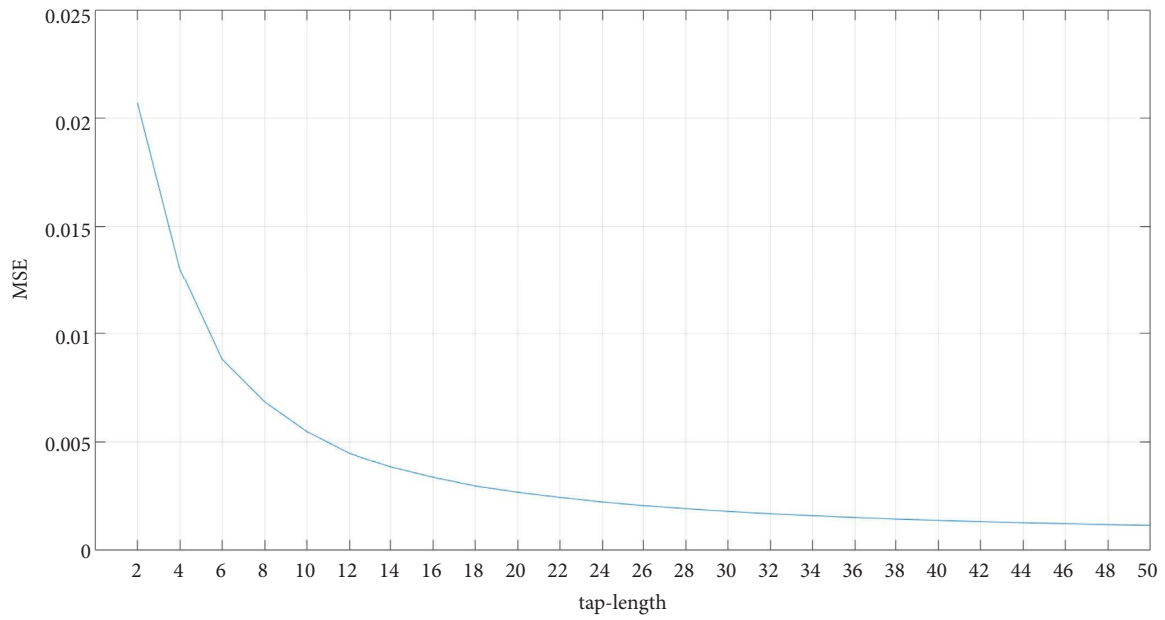
(c)
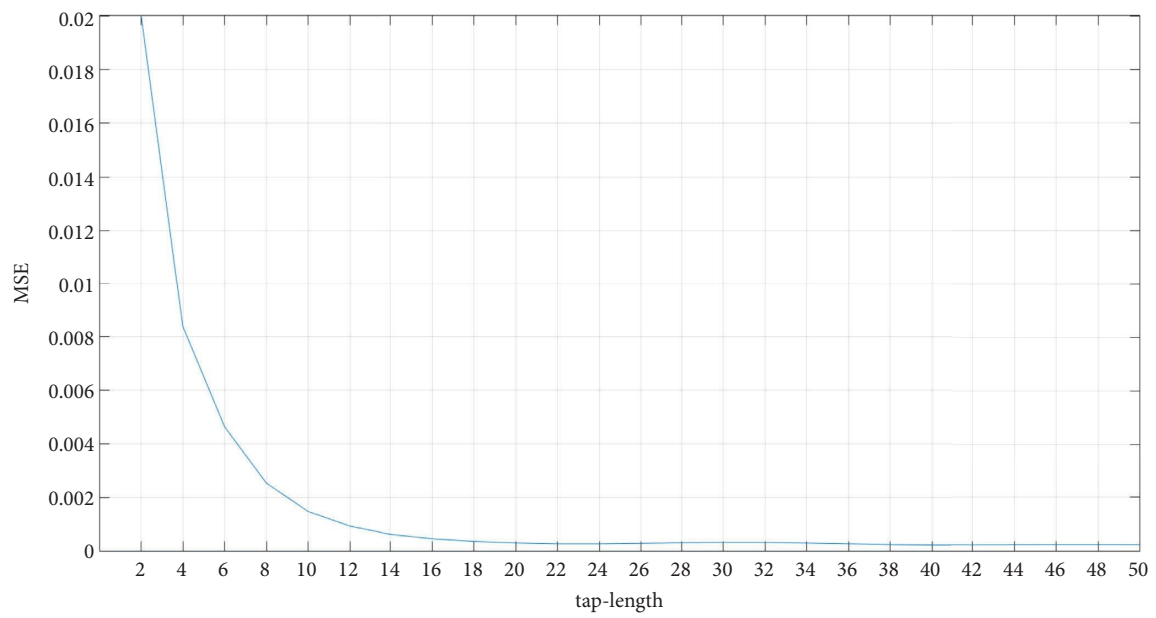
(d)

FIGURE 23: Continued.
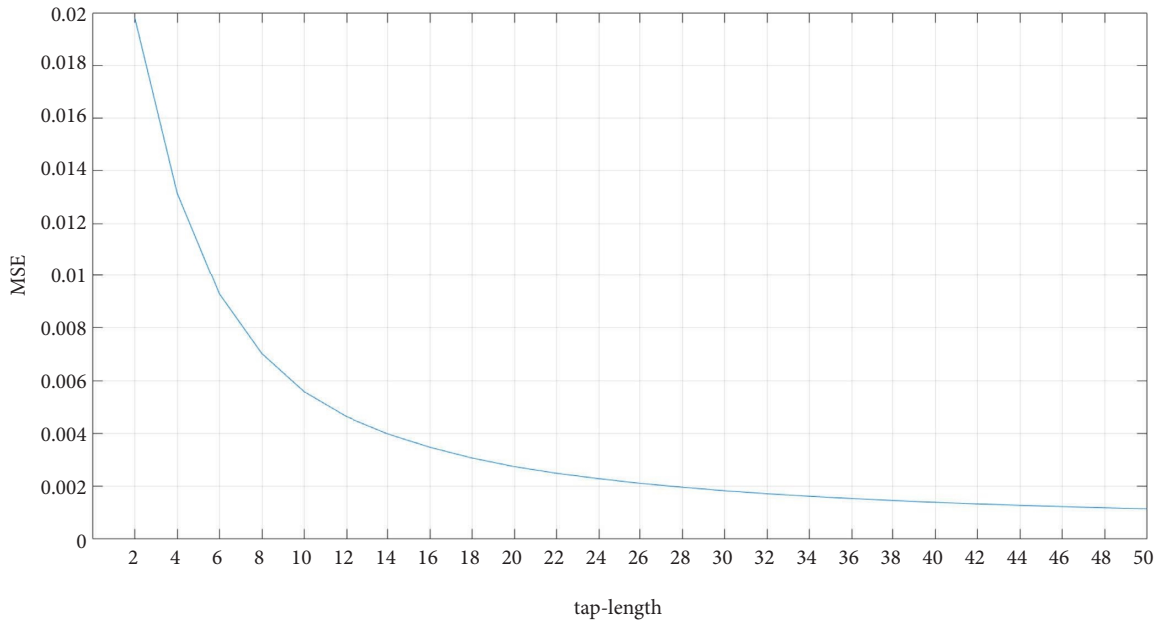
(e)
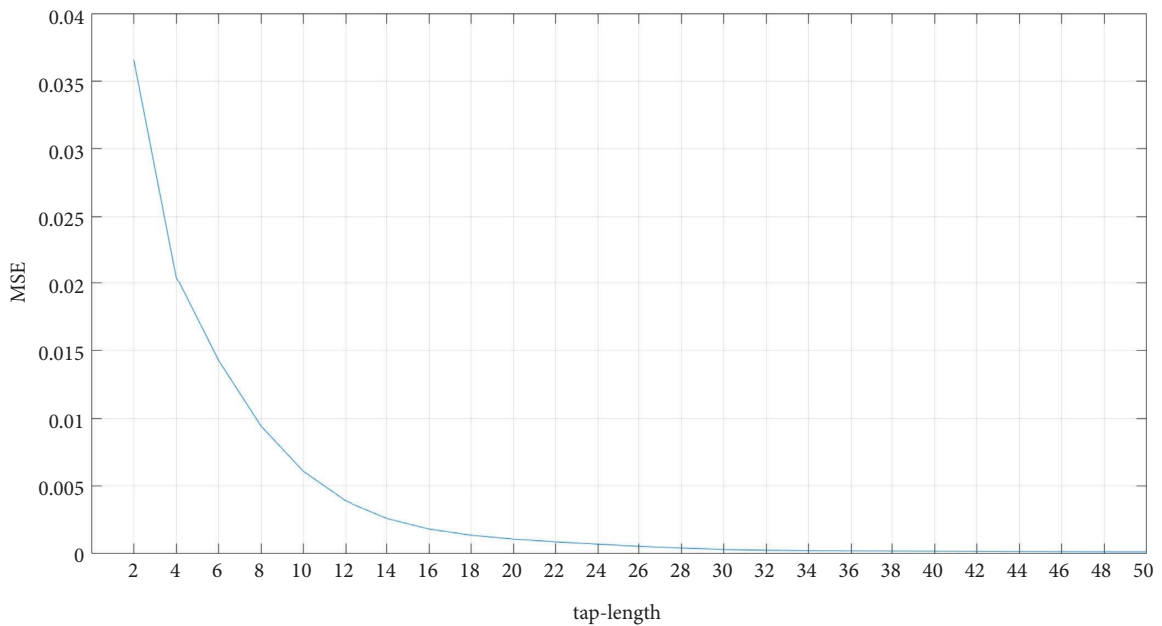
(f)

Figure 23: The diagrams of tap-length optimization. (a) LMS output MSE changing with tap-length for input torque at 1000 r/min. (b) LMS output MSE changing with tap-length for output torque at 1000 r/min. (c) LMS output MSE changing with tap-length for input torque at 2000 r/min. (d) LMS output MSE changing with tap-length for output torque at 2000 r/min. (e) LMS output MSE changing with tap-length for input torque at 3000 r/min. (f) LMS output MSE changing with tap-length for output torque at 3000 r/min.

Table 5: The optimum tap-length of LMS.

	Input torque at 1000 r/min	Output torque at 1000 r/min	Input torque at 2000 r/min	Output torque at 2000 r/min	Input torque at 3000 r/min	Output torque at 3000 r/min
LMS tap-length	36	20	40	18	40	20

For the mixed components of torque, the Kalman filter process is carried out to get rid of noise from the IMFs. The results processed by the Kalman filter are shown in Figure 21. According to the CMSE and ℓ2-norm calculating results, the noise components of IMFs are removed directly and the mixed components of IMFs are counted in; after

(a)

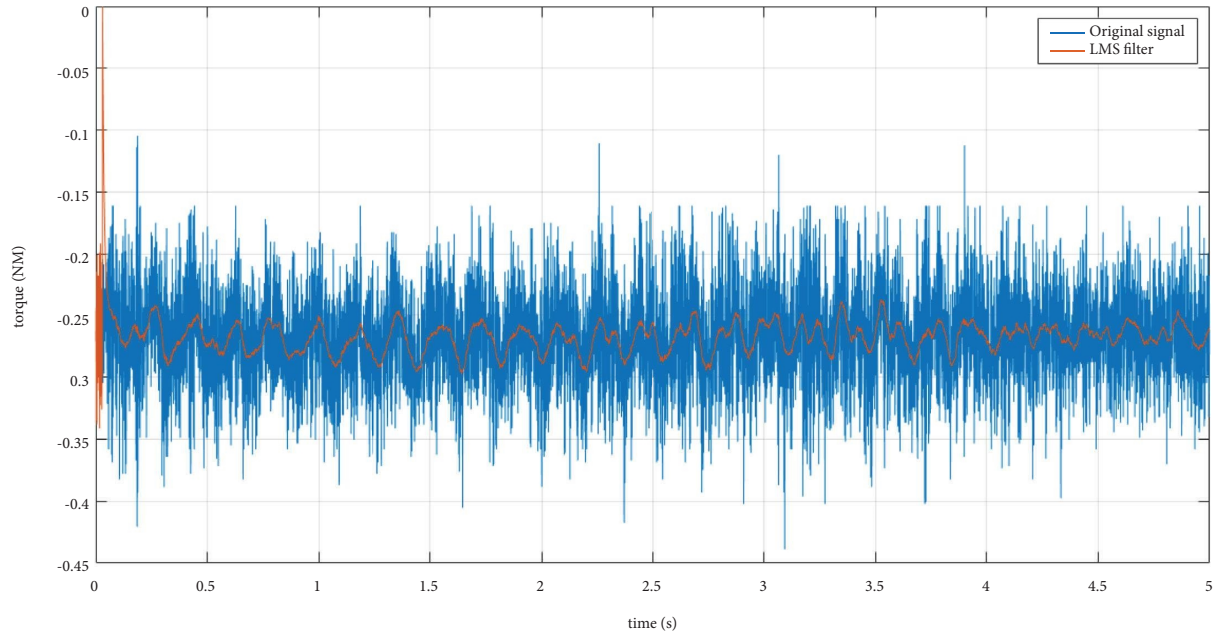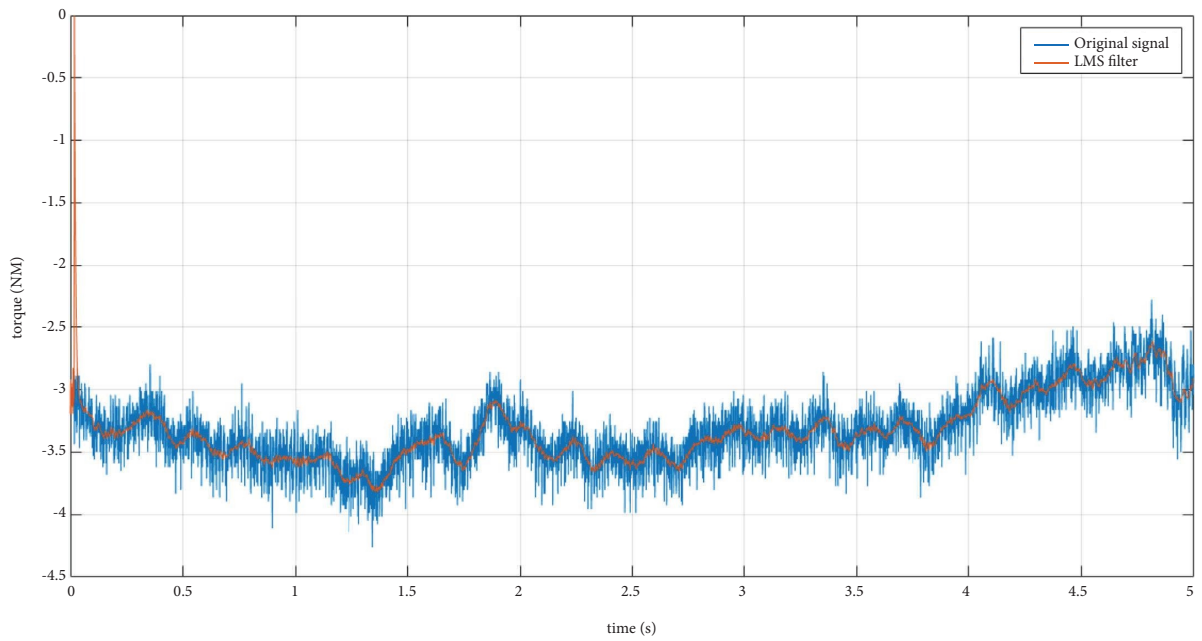
(b)

FIGURE 24: Continued.
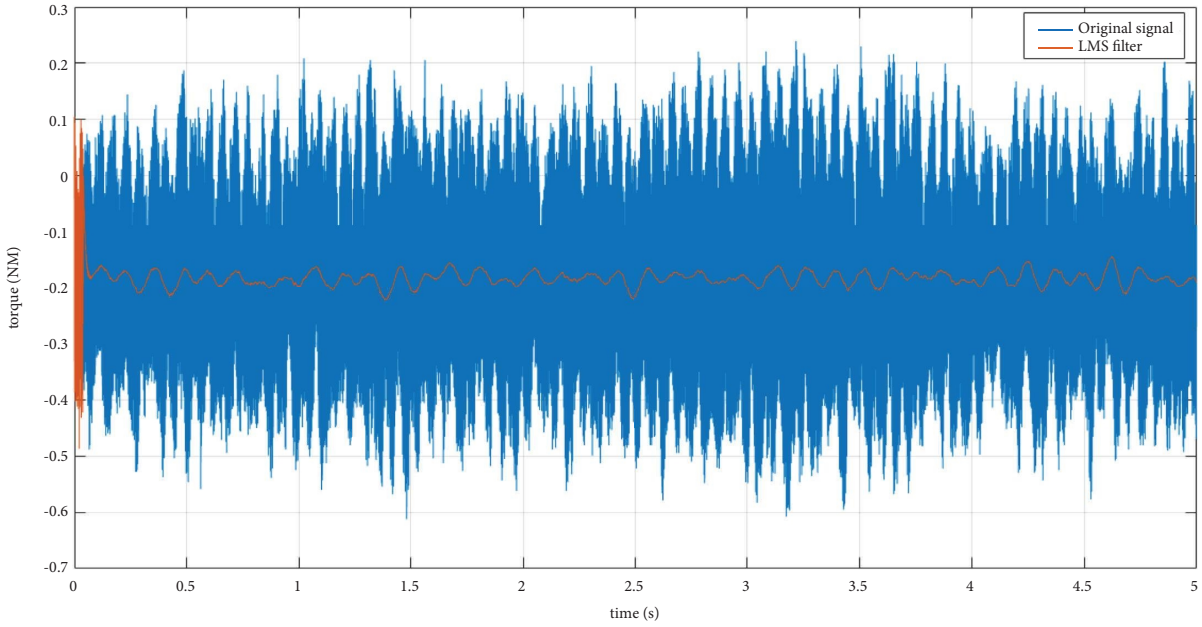
(c)
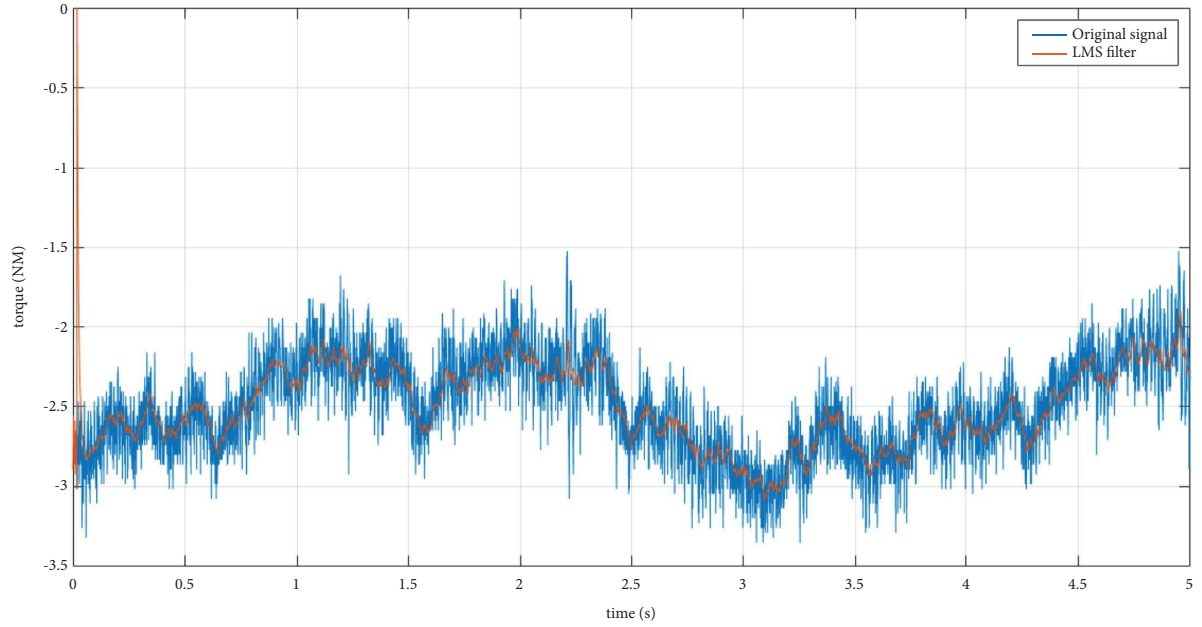
(d)

FIGURE 24: Continued.

(e)

(f)
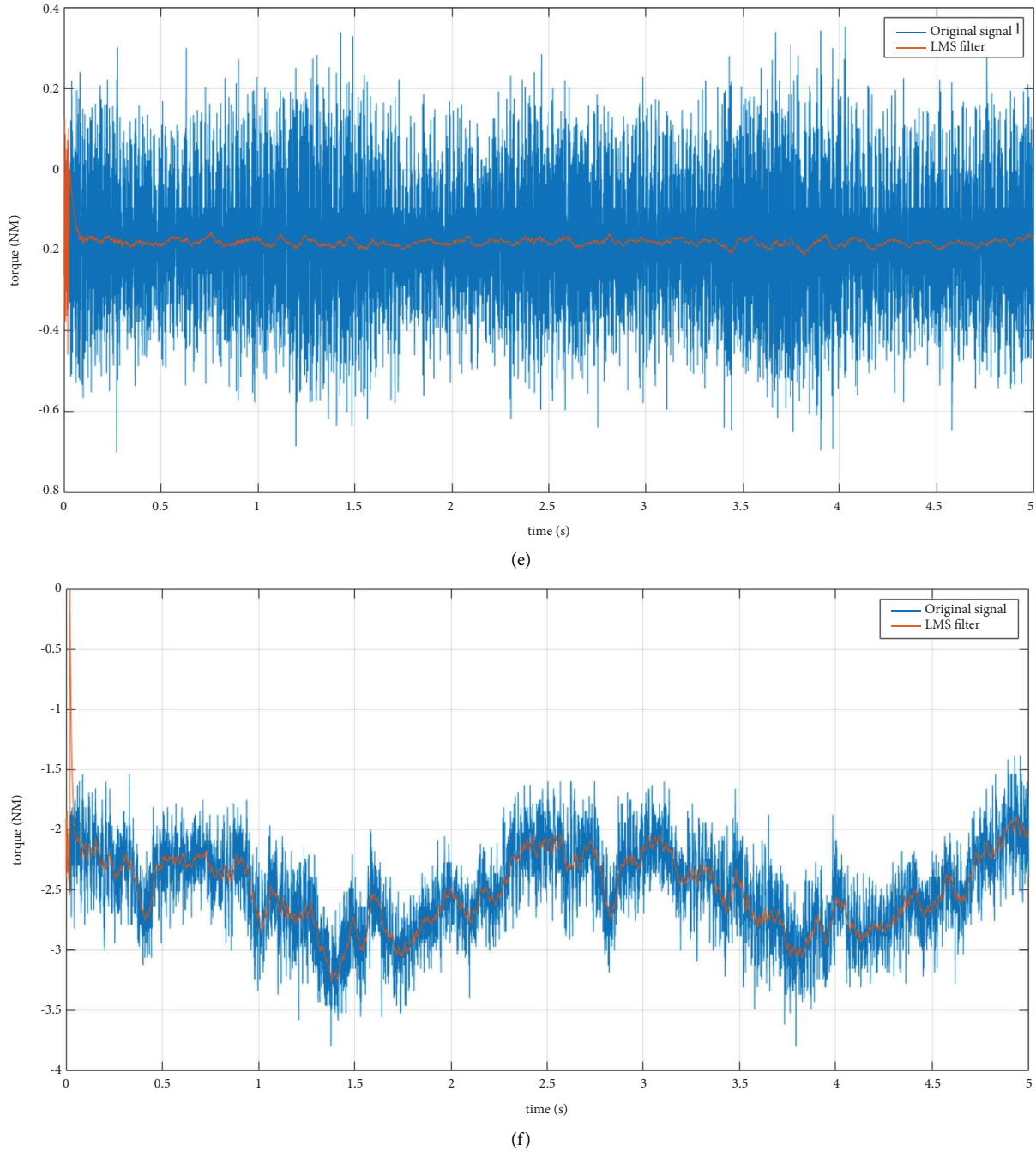
FIGURE 24: The results of LMS filter for torque. (a) The LMS filter of input torque at 1000 r/min. (b) The LMS filter of output torque at 1000 r/min. (c) The LMS filter of input torque at 2000 r/min. (d) The LMS filter of output torque at 2000 r/min. (e) The LMS filter of input torque at 3000 r/min. (f) The LMS filter of output torque at 3000 r/min.

the filter process is carried out by Kalman filter algorithm, the information components of IMFs are counted in directly, the results of reconstructed torque signals are shown in Figure 22. The SNR comparisons between original signal and denoised signal are shown in Table 4; the quality of signal is improved prominently by EMD algorithm. The outcomes of denoising torque signal are improved in the smoothness and stability, and the interference factors, such as sensor stochastic error and dynamic disturbance of couple, are depressed.

In the mechanical transmission, the motion parameters are requested to process in real-time, although EMD offers an effective approach to acquire denoised signal, the requirement of process in real-time is not satisfied, and the LMS combined with EMD can conquer disadvantages of EMD.

For calculating the optimum of tap-length, the MSE is used as index to evaluate, and the results are shown in Figure 23, and optimum of tap-length is shown in Table 5. The LMS algorithm is carried out, and the result is shown in Figure 24. The results indicate the LMS can appropriately

process no-denoised torque signal, the denoising error is narrow, and its effect can match with EMD algorithm, and LMS algorithm can fulfill denoising processing.

6. Discussion and Conclusion

Not only the core transmission facilities, such as RV reducer, but also the accurate kinetic parameter measurements are the critical factors in precise transmission. This paper focuses on the efficient approach to extract the more authentic signal from the transmission systems. The extraordinary advantages of EMD enable its outstanding power to processing signal, but non-instantaneous limitation restricts it to conduct online assignment. The combination between EMD and LMS is carried out, and the specific procedures are presented in this paper and illustrated in the simulation signal and experiment signals.

In the processing, the CMSE and ℓ2-norm are employed to discriminate the different components of IMFs. The EMD-PR strategy is applied in the denoising, the noise components of IMFs are discarded directly, the mixed components of IMFs will be counted in the reconstructed signal after being processed, and the information components will be used in the reconstruction directly. Different from the regular works of using threshold approach to denoising, the Kalman filter is applied in the denoising for mix components of IMFs. The reconstructed signal is used as reference signal in LMS processing. This hybrid approach can be evolved with different algorithms with different time-domain decomposition and different online filter methods.

The RV reducer experiments are carried out; kinetic parameters, rotation speed, and torque are measured in the experiments, especially the torque signal exists in amount of proportion of noise. The developed algorithm in this paper is conducted in simulation signal and mechanical transmission signal, and the EMD-LMS hybrid algorithm realizes high quality denoising.

Additionally, the proposed denoising approach possesses the ability to be applied to not only mechanical transmission but also other areas to process signal in time.

Data Availability

The data used to support the fndings of this study are available from the corresponding author upon request.

Conflicts of Interest

The authors declare that they have no conflicts of interest.

Acknowledgments

References

[1] A. D. Pham and H.-J. Ahn, "Rigid precision reducers for machining industrial robots," *International Journal of Precision Engineering and Manufacturing*, vol. 22, no. 8, pp. 1469–1486, 2021.

[2] X. Deng, S. Wang, L. Qian, and Y. Liu, "Simulation and experimental study of influences of shape of roller on the lubrication performance of precision speed reducer," *Engineering Applications of Computational Fluid Mechanics*, vol. 14, no. 1, pp. 1156–1172, 2020.

[3] L. Guo, Z. Wang, Y. Song, X. Shan, and D. Gan, "Structural optimization of a new type of lever-assisted gear reducer based on a genetic algorithm," *Mechanical Sciences*, vol. 12, no. 1, pp. 333–343, 2021.

[4] T. Hidaka, H. Wang, T. Ishida, K. Matsumoto, and M. Hashimoto, "Rotational transmission error of K-H-V planetary gears with cycloid gear. (lst Report.Analytical method of the rotational transmission error)," *Transactions Of The Japan Society Of Mechanical Engineers Series C*, vol. 60, no. 570, pp. 645–653, 1994.

[5] M. Blagojevic, N. Marjanovic, Z. Djordjevic, B. Stojanovic, and A. Disic, "A new design of a two-stage cycloidal speed reducer," *Journal of Mechanical Design*, vol. 133, no. 8, Article ID 085001, 2011.

[6] B. Chen, C. Peng, and J. Huang, "A new error model and compensation strategy of angle encoder in torsional characteristic measurement system," *Sensors*, vol. 19, no. 17, p. 3772, 2019.

[7] Y. Deng, Z. He, Y. Zhang, and S. Wang, "Synchronous monitoring of axial vibration and rotation speed of rotating cylinder by linear array scanning," *Mechanical Systems and Signal Processing*, vol. 181, Article ID 109445, 2022.

[8] Z. Yu, Z. Qiu, H. Li, J. Xue, and L. Zhao, "Measuring the no-load running torque of RV reducer based on the SVD and MCSA," *Measurement*, vol. 190, Article ID 110697, 2022.

[9] N. E. Huang, Z. Shen, S. R. Long et al., "The empirical mode decomposition and the Hilbert spectrum for nonlinear and non-stationary time series analysis," *Proceedings of the Royal Society of London Series A Mathematical Physical and Engineering Sciences*, vol. 454, no. 1971, pp. 903–995, 1998.

[10] N. E. Huang, "A new method for nonlinear and nonstationary time series: empirical mode decomposition and hilbert spectral analysis," *Wavelet Applications*, vol. 7, pp. 197–209, 2000.

[11] Y. Kopsinis and S. McLaughlin, "Development of EMD-based denoising methods inspired by wavelet thresholding," *IEEE Transactions on Signal Processing*, vol. 57, no. 4, pp. 1351–1362, 2009.

[12] H. Meng, F. Liu, and J. Qu, "Denoising algorithm of Φ_OTDR signal based on clear iterative EMD interval-thresholding," *Optics Communications*, vol. 453, pp. 1–7, 2019.

[13] G. Yang, Y. Liu, Y. Wang, and Z. Zhu, "EMD interval thresholding denoising based on similarity measure to select relevant modes," *Signal Processing*, vol. 109, pp. 95–109, 2015.

[14] A. Komaty, A.-O. Boudraa, B. Augier, and D. Daré-Emzivat, "EMD-based filtering using similarity measure between probability density functions of IMFs," *IEEE Transactions on Instrumentation and Measurement*, vol. 63, no. 1, pp. 27–34, 2014.

[15] X. Guo, C. Sun, P. Wang, and L. Huang, "Hybrid methods for MEMS gyro signal noise reduction with fast convergence rate and small steady-state error," *Sensors and Actuators A: Physical*, vol. 269, pp. 145–159, 2018.

[16] A. O. Boudraa and J. C. Cexus, "EMD-based signal filtering," *IEEE Transactions on Instrumentation and Measurement*, vol. 56, no. 6, pp. 2196–2202, 2007.

[17] A. Voznesensky and D. Kaplun, "Adaptive signal processing algorithms based on EMD and ITD," *IEEE Access*, vol. 7, pp. 171313–171321, 2019.

[18] A. Voznesensky, D. Butusov, V. Rybin, D. Kaplun, T. Karimov, and E. Nepomuceno, "Denoising chaotic signals using ensemble intrinsic time-scale decomposition," *IEEE Access*, vol. 10, pp. 115767–115775, 2022.

[19] B. Widrow and M. E. Hoff, "Adaptive switching circuits," *Nerocomputing-Foundations of Research*, vol. 12, pp. 96–104, 1960.

[20] D. Jin, J. Chen, C. Richard, and J. Chen, "Model-driven online parameter adjustment for zero-attracting LMS," *Signal Processing*, vol. 152, pp. 373–383, 2018.

[21] Z. Tang and B. Akin, "A new LMS algorithm based deadtime compensation method for PMSM FOC drives," *IEEE Transactions on Industry Applications*, vol. 54, no. 6, pp. 6472–6484, 2018.

[22] C. Lu, Z. Zheng, and S. Wang, "Degradation status recognition of axial piston pumps under variable conditions based on improved information Entropy and Gaussian mixture models," *Processes*, vol. 8, no. 9, p. 1084, 2020.

[23] H. Liu, X. Mi, and Y. Li, "An experimental investigation of three new hybrid wind speed forecasting models using multi-decomposing strategy and ELM algorithm," *Renewable Energy*, vol. 123, no. 8, pp. 694–705, 2018.

[24] Z. Wu and N. E. Huang, "Ensemble empirical mode decomposition: a noise-assisted data analysis method," *Advances in Adaptive Data Analysis*, vol. 1, no. 1, pp. 1–41, 2009.

[25] K. Chang and S. Liu, "Gaussian noise filtering from ECG by wiener filter and ensemble empirical mode decomposition," *Journal of Signal Processing Systems*, vol. 64, no. 2, pp. 249–264, 2011.

[26] X. Xie, S. Cheng, and X. Li, "Vibration diagnosis and optimization of industrial robot based on TPA and EMD methods," *Computer Modeling in Engineering and Sciences*, vol. 135, no. 3, pp. 2425–2448, 2023.

[27] Y. Qiao, M. Arabi, W. Xu, H. Zhang, and E. M. Abdel-Rahman, "The impact of thermal-noise on bifurcation MEMS sensors," *Mechanical Systems and Signal Processing*, vol. 161, Article ID 107941, 2021.

[28] C. Yin, Y. Wang, G. Ma, Y. Wang, Y. Sun, and Y. He, "Weak fault feature extraction of rolling bearings based on improved ensemble noise-reconstructed EMD and adaptive threshold denoising," *Mechanical Systems and Signal Processing*, vol. 171, Article ID 108834, 2022.

[29] A. Mert and A. Akan, "Detrended fluctuation thresholding for empirical mode decomposition based denoising," *Digital Signal Processing*, vol. 32, pp. 48–56, 2014.

[30] Y. Kopsinis and S. McLaughlin, "Empirical mode decomposition based soft-thresholding," in *Proceedings of the 2008 16th European Signal Processing Conference*, pp. 1–5, Lausanne, Switzerland, August 2008.

[31] S. Mallat, *A Wavelet Tour of Signal Processing*, Academic Press, San Diego, USA, 2nd edition, 1999.

[32] P. Flandrin, P. Gonçalvès, and R. Gabriel, *EMD Equivalent Filter banks, from Interpretation to Applications, Hilbert-Huang Transform and its Applications*, World Scientific Publishing, Hackensack, NJ, USA, 2nd edition, 2005.

[33] M. A. Z. Raja, N. I. Chaudhary, Z. Ahmed, A. Ur Rehman, and M. S. Aslam, "A novel application of kernel adaptive filtering algorithms for attenuation of noise interferences," *Neural Computing & Applications*, vol. 31, no. 12, pp. 9221–9240, 2019.

[34] Y.-H. Wang, C.-H. Yeh, H.-W. V. Young, K. Hu, and M.-T. Lo, "On the computational complexity of the empirical mode decomposition algorithm," *Physica A: Statistical Mechanics and Its Applications*, vol. 400, pp. 159–167, 2014.

[35] A. B. La Rosa, P. T. L. Pereira, P. Ücker et al., "Exploring NLMS-based adaptive filter hardware architectures for eliminating power line interference in EEG signals," *Circuits, Systems, and Signal Processing*, vol. 40, no. 7, pp. 3305–3337, 2021.